# Analysis of Linear Friction Welding of Dissimilar Metals: Aluminum and Copper with Zinc Interlayer

by

Sandesh Neupane

Submitted in Partial Fulfilment of the Requirements

for the Degree of

Master of Science in Engineering

in the

Mechanical Engineering Program

YOUNGSTOWN STATE UNIVERSITY

August 2023

Analysis of Linear Friction Welding of Dissimilar Metals: Aluminum and Copper with Zinc Interlayer

Sandesh Neupane

I hereby release this thesis to the public. I understand that this thesis will be made available from the OhioLINK ETD Center and the Maag Library Circulation Desk for public access. I also authorize the University or other individuals to make copies of this thesis as needed for scholarly research.

Signature:

*Sandesh Neupane*, Student Date

Approvals:

*Jae Joong Ryu PhD*, Thesis Advisor Date

*C. Virgil Solomon PhD*, Committee Member Date

*Kyosung Choo PhD*, Committee Member Date

Salvatore A. Sanders, PhD, Dean, College of Graduate Studies Date

# Abstract

This thesis presents an analysis of linear friction welding of dissimilar metals, specifically aluminum and copper, with a zinc interlayer. The welding of aluminum and copper is significant for heat transfer and electrical applications, as these metals are commonly used. Traditional fusion welding methods are ineffective due to the metals' differing melting points, making solid-state joining processes like friction welding preferable. The main objective of this research is to address the challenges in welding copper and aluminum using linear friction welding and to improve the strength of the resulting weld. One major issue encountered during welding is the formation of brittle intermetallic compounds at the interface. To overcome this problem, an interlayer of zinc is used during the welding process. This study investigates the impact of two different thicknesses of the zinc interlayer, namely 0.07 mm and 0.2 mm.

The welding process was conducted using a 20-ton vertical oscillator welding machine. The resulting welds were subjected to various analyses, including tensile tests, hardness tests, scanning electron microscopy (SEM), and energy-dispersive X-ray spectroscopy (EDS). Successful welding was achieved both with and without the interlayer. There was no significant difference in the ultimate tensile strength (UTS) between the two interlayer thicknesses, but the UTS of the samples with interlayers showed a 28% increase compared to the samples without interlayers. The hardness at the junction without an interlayer was higher (180 HV) than the hardness with an interlayer (159 HV). SEM images revealed cracks in the welding regions without interlayers, indicating the formation of brittle intermetallic compounds at the junction.

Thermal analysis was also performed to predict the temperature at the junction during welding, utilizing parameters such as frequency, amplitude, and time.

The use of interlayer materials was found to enhance the tensile strength of the weld while reducing the hardness at the junction, suggesting a decrease in the formation of brittle intermetallic compounds. The thermal analysis successfully predicted the junction temperature. Further improvement could be achieved by optimizing parameters such as initial pressure, forge pressure, amplitude, and frequency. Additionally, comprehensive thermal analysis, considering heat conduction from the specimen to the tooling, can offer a deeper understanding of the welding process. Future experiments should incorporate the assumptions made in this study to further enhance the outcomes of copper-aluminum friction welding. These proposed enhancements pave the way for achieving stronger and more reliable joints in the future.

# Acknowledgements

I would like to express my sincere gratitude to the individuals who have contributed to the completion of this thesis. First and foremost, I would like to extend my deepest appreciation to my thesis advisor, Dr. Jae Joong Ryu. His expertise, dedication, and unwavering support have been instrumental in shaping this thesis. I am grateful for his guidance, insightful feedback, and encouragement, which have pushed me to explore new frontiers and strive for excellence.

I would also like to thank the members of my thesis committee, Dr. C. Virgil Solomon, for his guidance in mechanical testing and microstructure analysis, and Dr. Kyosung Choo, for his expert advice on heat transfer analysis during welding. Their expertise and critical insights have immensely improved the quality of this work.

I am grateful to Mr. Mike Gaskill and Taylor Winfield for their generous support in providing the necessary equipment for friction welding. Their contribution has enabled me to conduct experiments efficiently and effectively.

I am indebted to Dr. Bharat Yelamanchi for his assistance with the hardness tests conducted in this study. Special thanks are extended to Mr. Ray Hoff and Mr. Ibrahim Khalilullah for their help in SEM and EDS analysis.

I would like to express my heartfelt appreciation to my loving wife, Ashmita, for her continuous emotional support throughout the experiment. Additionally, I would like to show my gratitude to my friends, Saroj, Mukesh, Niyam, Sahaj and Sushant for their continuous support throughout my academic journey.

# List of Figure

# List of Table

# Nomenclature

| | |
|---|---|
| LFW | Linear Friction Welding |
| Al | Aluminum |
| Cu | Copper |
| Zn | Zinc |
| σ | Normal stress |
| HAZ | Heat Affected Zone |
| FSSW | Friction Stir Spot Welding |
| CSA | Cross Section Area |
| F | Force |
| A | Area |
| SEM | Scanning Electron Microscope |
| EDS | Energy-dispersive X-ray spectroscopy |
| GPa | Giga Pascal |
| MPa | Mega Pascal |
| UTS | Ultimate Tensile Strength |

# Table of Contents

# 1 Introduction

## 1.1 Background of the Study

Humans have been using metals for thousands of years. People use metals like copper, iron, and bronze for various purposes, including tool making, weapon making, and construction. The use of metals and metallurgy has played a central role in human civilization and technology, with advances in metallurgy leading to the development of new alloys and materials.[1]

Different metals have different properties and different metals are used for specific purposes. For instance, steel is often used in construction and manufacturing due to its strength and durability. Aluminum, on the other hand, is lightweight and has good conductivity, making it a popular choice for electrical wiring and in the aerospace industry. Copper is highly conductive and is commonly used in electrical wiring and in the production of coins and jewelry. Gold is non-reactive and has a high resistance to corrosion, making it a popular choice for jewelry and coins. These properties, along with cost and availability, determine which metals are used for specific applications. The combination of two or more metals can lead to the creation of alloys with unique properties, such as increased strength, improved corrosion resistance, or enhanced electrical conductivity.

Copper and aluminum are two widely used materials in the industry due to their unique properties and versatility. Copper is known for its high thermal and electrical conductivity, while aluminum is valued for its strength-to-weight ratio and resistance to corrosion. Copper is used in a variety of applications such as electrical wiring, plumbing, and roofing materials, among others [3]. Copper is also used in the construction of power generation and transmission systems,

industrial machinery, and electronic devices. Aluminum, on the other hand, is widely used in the construction, transportation, and packaging industries due to its lightweight and corrosion-resistant properties [3]. Aluminum is used in the production of aircraft and automobiles, as well as in the manufacturing of cans, foils, and other packaging materials. The versatility of aluminum also makes it a valuable material in the construction of buildings, including doors, windows, and facades [4]. Some of the common properties between copper and aluminum are they both have high thermal conductivity ( $398\,W/m-K$ for copper and $210\,W/m-K$ for aluminum) and electrical resistivity ($1.7\times10^{-6}ohm-cm$ for copper and $2.7\times10^{-6}\,ohm-cm$) [5]. Such common properties can be used in the common application in electronics, thermos-techniques, and other areas, in the form of bimetals.

Traditional Fusion welding is not effective for joining dissimilar metals because of their different thermal properties like melting points and thermal diffusivity. So, there is a technique to join those dissimilar metals with solid state joining process. Friction welding is one of the widely used solid state joining process. Friction welding does not require a filler material, and the welded joint is formed by the mechanical deformation and fusion of the parent materials. Due to this reason, friction welding has been very good option for joining dissimilar metals, such as copper and aluminum, which are difficult to join using other welding methods [2]. So, this experiment is to conduct the friction welding between copper and aluminum and to find the ways to improve the weld.

## 1.2 Problem statement and research objectives

Although Aluminum and Copper have some comparatively similar properties like thermal conductivity and electrical conductivity, they have different mechanical and physical properties. Due to these reasons welding of those two metals comes with challenges. One of the main challenges while joining copper and aluminum with the traditional fusion welding is the difference in melting points. Copper has higher melting point (1084°C) than aluminum (660°C), this makes it difficult to melt both metals at the same time without overheating and one metal and underheating the other.[6] Another issue with the aluminum and copper welding is that they have different physical and metallurgical properties. Copper has slightly higher thermal conductivity than aluminum, which makes it difficult to maintain a uniform heat distribution during the welding process. [6] Another challenge is the formation of intermetallic compounds at the interface of the two materials. Those intermetallic compounds are brittle and have a negative impact on the mechanical properties of the joint, including reduced strength and ductility. Intermetallic compounds weaken the joint and make it susceptible to cracking and failure.[7]

The objective of the research is to overcome the problem of traditionally welding copper and aluminum with linear friction welding and finding the ways to improve the strength of the weld. Friction Welding is a solid-state joining process that has gained increasing popularity in the manufacturing industry due to its advantages over traditional fusion welding methods [2]. One type of friction welding is linear friction welding (LFW), which is a forging process that can produce high-strength joints with excellent repeatability and minimal or no heat-affected zone (HAZ) [2].

Linear friction welding is achieved due to the high temperature and the pressure at the interface. Since aluminum and copper have different melting points, thermal conductivity, and coefficients of thermal expansion, there are challenges to join those two materials. Interlayer materials, such as Zinc are often used in friction welding to improve the properties of the joints and to mitigate these challenges [11].

The aim of this study is to analyze the linear friction welding of copper and aluminum with and without the interlayer materials, with the focus on the properties of the resulting joints. This research is motivated by the need to understand the influence of interlayer materials on the friction welding process and to provide insights into the feasibility of using LFW as a joining method for copper and aluminum.

## 1.3 Significance and contribution of the Study

The significance of this study lies in its contribution to the understanding of the influence of interlayer materials on the linear friction welding of copper and aluminum. This research will provide important insights into the feasibility of using LFW as a joining method for these two materials.

The results of this study will provide practical information for industry professionals and researchers in the field of welding and materials science. The findings of this study will be useful for the development of new joining methods for copper and aluminum, and for the optimization of the linear friction welding process with interlayer materials.

Furthermore, this research will contribute to the existing literature on friction welding and the use of interlayer materials in solid-state joining processes [2]. The results of this study will provide a basis for future studies in this field and will help to advance the understanding of the properties and behavior of copper and aluminum joints produced by LFW with interlayer materials.

This study will not include a comprehensive review of all types of friction welding or a detailed examination of the other interlayer materials that can be used in friction welding. The focus of this research is to understand the influence of interlayer materials on the linear friction welding of copper and aluminum.

# 2 Literature Review

## 2.1 Overview of Friction Welding

Friction welding is a solid-state joining process that uses friction and pressure to generate heat and fuse two components together. Unlike traditional welding processes, friction welding does not require a filler material, and the welded joint is formed by the mechanical deformation and fusion of the parent materials. This makes friction welding an attractive option for joining dissimilar materials, such as copper and aluminum, that are difficult to join using other welding methods [2].

There are different types of friction welding techniques used in various industries. One of the most common friction welding techniques is rotary friction welding. In rotary friction welding, one component is rotated against the other component, generating friction and heat. The heat generated during the friction process causes the material at the interface to soften and deform, forming a forging region that is compressed by the clamping force. The forging region is then cooled and solidified, forming a metallurgical bond between the two components [2]. Another type is linear friction welding, which uses a reciprocating motion to create friction and heat between the two components until they are bonded together. A third type is friction stir welding that uses a rotating tool to create heat and friction between two components, which are then bonded together through plastic deformation [9].

## 2.2 Linear Friction Welding

Linear friction welding (LFW) is a variation of friction welding that involves a linear motion of one component against the other component, as opposed to a rotary motion. In LFW, the relative motion between the components is generated by a linear movement of one component along a straight line, while the other component is stationary [12]. LFW has several advantages over other friction welding methods, including higher welding speed, improved welding accuracy, and the ability to join longer and thicker components [12]. LFW is also capable of producing high-quality welds with uniform microstructures and good mechanical properties [11].

## 2.3 Interlayer Materials in Friction Welding

The use of interlayer materials in friction welding is a widely studied and applied method for improving the properties of the welded joints. Interlayer materials can be used to enhance the interfacial bonding between the components, reduce the formation of oxides at the interface, and improve the formation of the forging region during the welding process [11].

Interlayer materials have been previously used in different friction welding of other dissimilar materials, such as steel and aluminum, and have been found to improve the bonding and mechanical properties of the welded joints [10]. For example, nickel has been found to be an effective interlayer material for friction welding of steel and aluminum, as it has high thermal conductivity, good wettability with both steel and aluminum, and low thermal expansion coefficient [10].

In friction welding of dissimilar metals, such as copper and aluminum, the interlayer material can be used to overcome the mismatch in the thermal expansion coefficients and improve the mechanical properties of the welded joints [4]. For example, zinc has been found to be an effective interlayer material for friction welding of copper and aluminum, as it has a low melting point, good wettability with both copper and aluminum, and low thermal expansion coefficient [11].

## 2.4 Previous studies on Copper-Aluminum Friction Welding

There are various studies that investigate the properties of friction welded copper-aluminum. Bekir S. Yilbas et al., (1993) investigated the mechanical and metallurgical properties of friction-welded aluminum-copper bars. It was found that the individual effect of main parameters such as speed of rotation, friction pressure and duration of welding have less significant in strength properties. However, the interactions of those main parameters have a significant effect on the mechanical strength of the welded region [17]. Laudern A.R. et al., (1973) demonstrated that contaminations such as grease at the welded surface reduce the quality of welded joint [18]. So, it is important to remove any contamination present at the welding surface before performing the welding. Bhamji I. et al. (2012) conducted linear friction welding to see the electrical resistivity across the weld. The formation of intermetallic compounds such as $Cu_2Al$, $Cu_3Al_2$, $Cu_4Al_3$ etc. significantly decrease the electrical conductivity across the weld [19]. Bhamji and his peers also conducted the tensile test and hardness test on the sample. On these tensile tests, fracture was observed on parent material away from the weld line which suggest that the weld region has the higher tensile strength than the parent aluminum [19]. It was also seen that the hardness increases towards the welding region as measured along one parent material to other across the weld [19].

Chapke Y. et al. (2020) also conducted the rotary friction welding on aluminum alloy 6063 with copper. It was found that the less friction time forms the inadequate IMC layer which resulted in failed friction weld joints [20]. Chapke Y, et al. (2020) were able to obtain a UTS of 222.787 MPa which was greater than previous research work. It was also concluded that the strength of the welded joint increased with the increase in friction time and upset pressure [20]. Boucherit A. et al. (2017) conducted the FSSW of AL and Cu with zinc interlayer to see the effect of Zn interlayer in the welding. It was found that the in presence of Zn interlayer, the strength and fracture energy of the joints are improved. However, there was still formation of IMCs. The thickness of the interlayer does not affect the strength of the weld [22]. Ratkovic N R. et al. (2016) examined the influence of parameters on the properties of the Al-Cu joint. Parameters such as friction time, friction pressure and contacting pressure were analyzed to see the mechanical and microstructural characteristics of the weld. It was found that friction speed within the range of small angular velocities, the joints are of good quality and at large speed, the joints are of poor quality. It was concluded that the increase in welding time increases the tensile strength of the joint. The hardness near the welded joint was found to be 130 HV [23]. Sahin M. (2009) conducted the experiment for joining copper and aluminum by friction welding. It was found that the welded zone has maximum tensile strength of 140.12 MPa with a friction pressure of 60 MPa and friction time of 2.5 seconds. It was also seen that the aluminum side has more axial shortening than the copper side. Contrary to other similar research, this research showed that the hardness decreases as towards the welded joints as moving from one parent material to another [24].

# 3 Research Methodology

This research will employ an experimental approach, utilizing a 20-ton vertical oscillator linear friction welding machine capable of joining copper and aluminum specimens. The process parameters including frequency, axial pressure, and forging time was varied to get the successful weld. Successful weld was then tested to find the mechanical properties like tensile strength, hardness test. The LFW joints were sectioned and prepared for microstructural analysis. Scanning electron microscopy (SEM), and energy-dispersive X-ray spectroscopy (EDS) was employed to examine the microstructure and to determine the nature of the fracture.

## 3.1 Materials and Equipment

### 3.1.1 Copper and Aluminum Sample

For the experiment, aluminum used in study was 6061 alloy and copper used us commercially found pure copper which were ordered from McMaster Car. Copper and Aluminum sample was obtained as a $304.5\,mm \times 304.5\,mm$ slab which was cut into $63.5\,mm \times 88.9\,mm$ slab that was used for the friction welding. Sample was cut into small slabs by using the pencil cutter.

Table 3-1 and 3-2 show the chemical composition of the aluminum and copper specimen used in friction welding.

*Table 3-1: Chemical Composition of Aluminum Specimen.*

| Element | Al | Si | Fe | Cu | Mn | Mg | Zn | Cr | Ti |
|---|---|---|---|---|---|---|---|---|---|
| % | 97.961 | 0.596 | 0.424 | 0.092 | 0.094 | 0.568 | 0.033 | 0.009 | 0.021 |

*Table 3-2: Chemical Composition of Copper Specimen.*

| **Element** | **Cu** | **Si** | **P** |
|---|---|---|---|
| **%** | 99.987 | 0.007 | 0.006 |

Physical properties of aluminum and copper is summarized in Table 3-3 below:

*Table 3-3:Properties of Aluminum and Copper.*

| Property | **Aluminum** | **Copper** |
|---|---|---|
| **Density** $(Kg/m^3)$ | 2710 | 8960 |
| **Melting Point** $(°C)$ | 660 | 1083 |
| **Young's Modulus** $(GPa)$ | 68.9 | 117 |
| **Thermal Conductivity**$(W/mK)$ | 210 | 398 |
| **Yield Strength** $(MPa)$ | 276 | 83 |
| **Ultimate Strength** $(MPa)$ | 310 | 170 |
| **Elongation at Break** (%) | 12-17 | 12 |

### 3.1.2 Interlayer Material

Various thicknesses of zinc were used as an interlayer during the LFW. Among those most of the thickness were not compatible while welding due to inadequate pressure because of limitation of the welding machine. Physical properties of Zinc are summarized in Table 3-4.

*Table 3-4: Physical Properties of Zinc.*

| **Property** | **Zinc** |
|---|---|
| **Density** $(Kg/m^3)$ | 7100 |
| **Melting Point** $(°C)$ | 420 |
| **Young's Modulus** $(GPa)$ | 96.5 |
| **Thermal Conductivity**$(W/mK)$ | 112.2 |
| **Yield Strength** $(MPa)$ | 75 |
| **Ultimate Strength** $(MPa)$ | 90 |

### 3.1.3 Linear Friction Welding Machine

For the LFW, vertical oscillation welder was used from Taylor Winfield which is shown in Figure 3-1. This equipment is a 20-ton vertical oscillation welder, and it doesn't have a formal model number as it was customized for Taylor Winfield. It can oscillate in a wide range of frequency up to 100 Hz. This equipment comes with the technology that can pre-heat the metal pieces before welding to avoid sudden change of temperature. For the sample with cross section of $63.5\ mm \times 88.9\ mm$ equipment could not provide enough pressure, so the cross section was decreased by $75\%$ to get the enough pressure at the junction during welding.

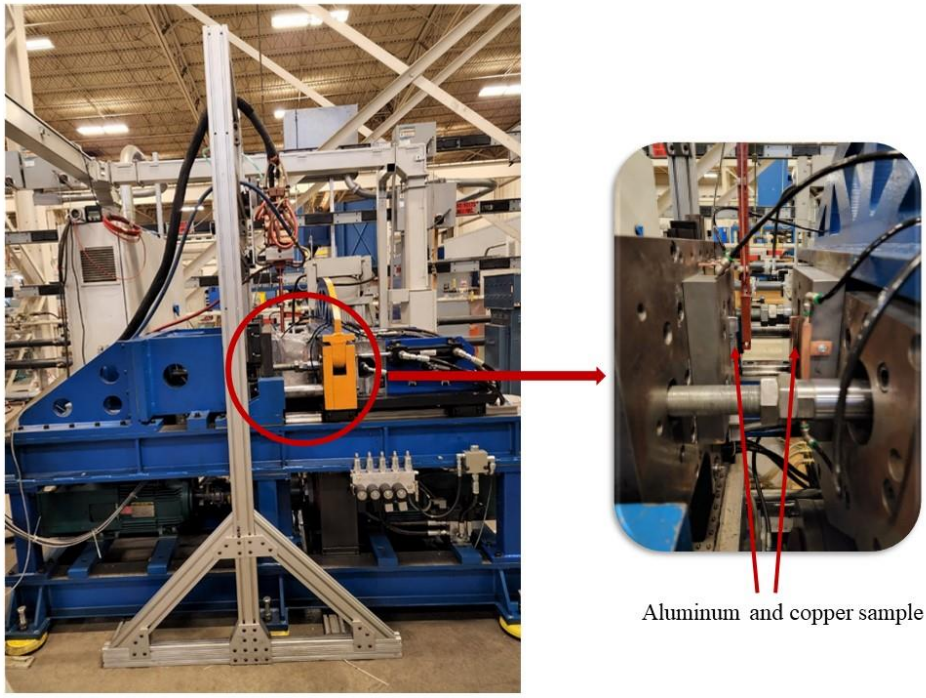


*Figure 3-1: 20-ton vertical oscillator welding machine.*

## 3.2 Sample Preparation

Copper and Aluminum specimen was ordered from the McMaster Car, and it was in the form of $304.5\,mm \times 304.5\,mm$ slab. Specimen was cut into small $63.5\,mm \times 88.9\,mm$ pieces using the pencil cutter available at one of the labs at Youngstown State University. Sample had thickness of $6.35\,mm$. Initial sample with cross section of $63.5\,mm \times 88.9\,mm$ was too big to develop enough pressure at the interface so the sample was cut in such a way that the cross section of the welding interface was $75\%$ less than the original sample. Figure 3-2 shows the shape of the sample that was used for the welding. Sample shown in Figure 3-2 (a) was not able to weld due to the larger surface area at the interface. Sample shown in Figure 3-2 (b) was cut in such a way so that there is enough pressure developed at the interface. However, there was development of clockwise moment at the protrude section due to asymmetry. So, the sample was cut as a shape shown in Figure 3-2 (c) to avoid the moment developed on the sample.

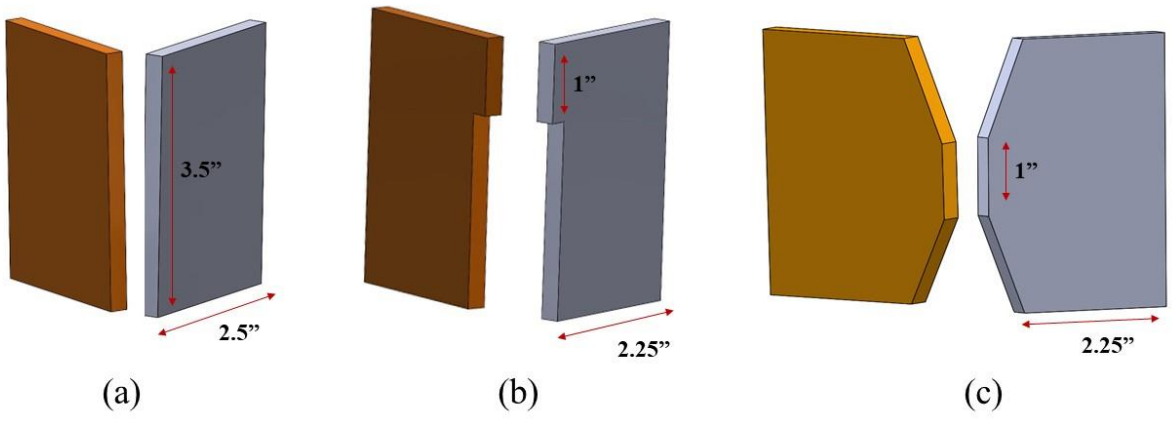


*Figure 3-2: Evolution of welding samples.*

Once the sample was cut into the shape shown in Figure 3-2 (c) the sample was welded with linear friction welding. During welding, the sample had an uneven surface at the interface due to the flash. Sample was polished at the interface to remove the uneven surface, which was then used for the tensile test, nano indentation, and microscopy. Both unpolished and polished welded samples are shown in Figure 3-3(a) and Figure 3-3(b) respectively.

(a) (b)

*Figure 3-3: (a) Unpolished and (b)Polished Welded Sample.*

The polished welded sample shown in Figure 3-3 (b) had a sharp corner at the interface which would act as a stress concentration during tensile test, so it was milled to have a circular interface as shown in Figure 3-4. The radius of the circular notch was $9.525\ mm$ keeping the welding section of $44.45\ mm$.

*Figure 3-4: Welded sample with notch for tensile test.*

For nano indentation, a rectangular sample was prepared and was polished to make the surface smooth. Cutter from one of the labs from Youngstown State University to cut the sample. Sample was cut far enough from the welded region so that there is no effect of heat at the welded interface as shown in Figure 3-5.

*Figure 3-5: Polished sample for nano indentation and microscopy.*

## 3.3 Welding process and parameters

The selection of the welding parameters, including the welding speed, applied load, and the duration of the forging region, has a significant impact on the quality of the LFW welds [13]. Welding parameters such as initial pressure, forging pressure, frequency, amplitude during the welding play a significant role in quality of the weld. Those parameters define the temperature at the junction during welding and the burn off distance of the sample. L. Zhou et al. in their research on rotary friction welding concluded that the rotational speed is the dominant parameter and studied the effect of rotational speed on mechanical properties [21]. Finding the right parameter for the welding was one of the main challenges for the project. Various parameters were used during different trials to weld copper and aluminum. Only the combination of right parameters was able to produce the good quality weld.

### 3.3.1 Trial 1

For the first trial sample with cross section with $63.5\ mm \times 88.9\ mm$ was used. Due to the limitation of the friction welding machine, only the pressure of 45 MPa was applied during the welding. 45 MPa was not enough for friction welding which results in failed welding. Figure 3-6 shows the failed welding and Table 3-5 shows the parameter used during welding.

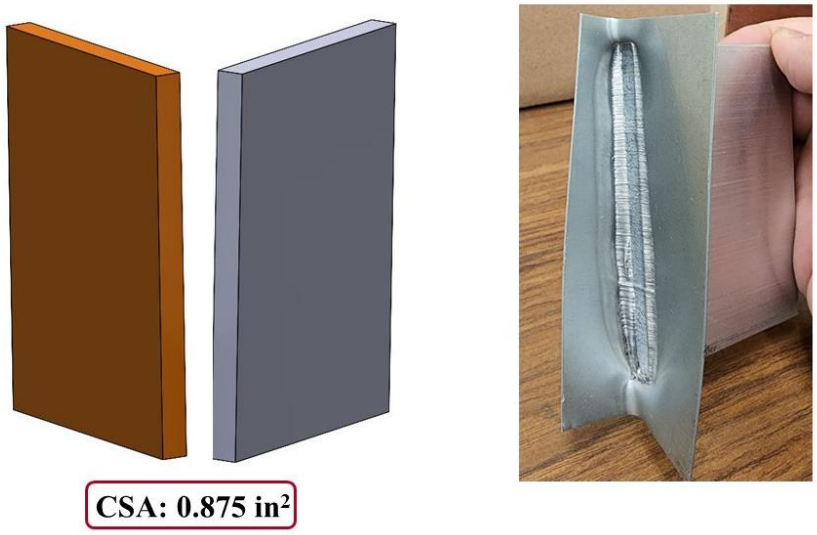


*Figure 3-6: Failed welding Trial 1.*

*Table 3-5: Parameters used during Trial 1.*

| Pressure (MPa) | Forge Pressure (MPa) | Frequency (Hz) | Amplitude (mm) |
|---|---|---|---|
| 45 | 45 | 50 | 0.5 |

### 3.3.2 Trial 2

To increase the pressure at the interface, the cross section of the sample was decreased by 75% for the second trial. However, due to the shape of the sample, there was a clockwise moment developed on the protruded section due to the higher pressure and the welding was unsuccessful. Figure 3-7 shows the shape of the sample and unsuccessful weld. Table 3-6 shows the parameters used during welding.

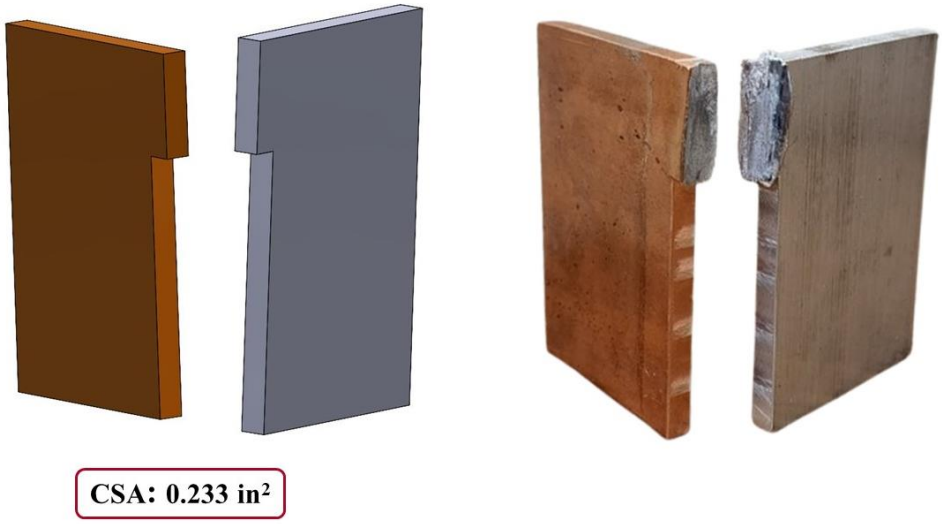


*Figure 3-7: Failed Welding Trial 2.*

*Table 3-6: Parameter used during Trial 2.*

| Pressure (MPa) | Forge Pressure (MPa) | Frequency (Hz) | Amplitude (mm) |
|---|---|---|---|
| 83 | 96 | 50 | 0.02 |

### 3.3.3 Trial 3 (Without Interlayer)

Specimen with the same shape as Trial 2 was used in Trial 3 but without the interlayer. For this trial pressure was slightly decreased to avoid the bending moment at the protruded section. Successful welding was obtained during this trial. However, the welded sample had cracks at the interface while viewing under microscope. Figure 3-8 shows the shape of the sample and successful weld and Table 3-7 shows the parameter used during welding.


*Figure 3-8: Successful welding Trial 3.*

*Table 3-7: Parameters used in Trial 3.*

| Pressure (MPa) | Forge Pressure (MPa) | Frequency (Hz) | Amplitude (mm) |
|---|---|---|---|
| 65 | 65 | 50 | 0.5 |

### 3.3.4 Trial 4

For this Trial, specimen was cut into different shape than the Trial 2 and 3 to avoid the bending moment. Higher pressure could be applied to the specimen with this shape. Success welding was obtained with this trial. During this trial multiple specimens were welded with different pressure ranging from 100 MPa to 200 MPa. With all the pressure, a successful welding was obtained. There was no significant change in tensile strength with change in welding pressure. Figure 3-9 shows the shape of the sample and successfully welded sample. Table 3-8 shows the parameters used during this trial.


*Figure 3-9: Successful Welding Trial 4.*

*Table 3-8: Parameters used in Trial 4.*

| Pressure (MPa) | Forge Pressure (MPa) | Frequency (Hz) | Amplitude (mm) |
|---|---|---|---|
| 100-200 | 100-200 | 50/60 | 0.5 |

## 3.4 Characterization and Analysis

Once the successful welding was obtained, the samples were first visually inspected to see if there were any visible cracks present in the welding region. Once the visual inspection was done, there were no sign of cracks on the welding region. The specimen was further viewed under VHX digital microscope as shown in Figure 3-10 to look for the cracks.


*Figure 3-10: VHX digital microscope.*

### 3.4.1 Tensile test

To determine the strength of the welded sample, tensile testing was done. Tensile testing was done using the Instron 5500R machine as shown in Figure 3-12. For the tensile test sample was cut as shown in Figure 3-4 to remove any stress concentration factor due to the sharp edges at the welded junction. The radius of the circular notch was 9.525 mm keeping the welding section of 44.45 mm. The loading rate for the tensile test was 1.5 mm/min. For the tensile test, gauge length was 50.8 mm. To calculate the stress, the cross-section area was normalized to find the nominal stress. However, since there is a notch which acts as a stress concentration factor, actual stress was greater than the measured stress during the tensile test. To find the actual stress, stress concentration factor was to be determined. Stress concentration factor was determined based on the chart shown in Figure 3-11.

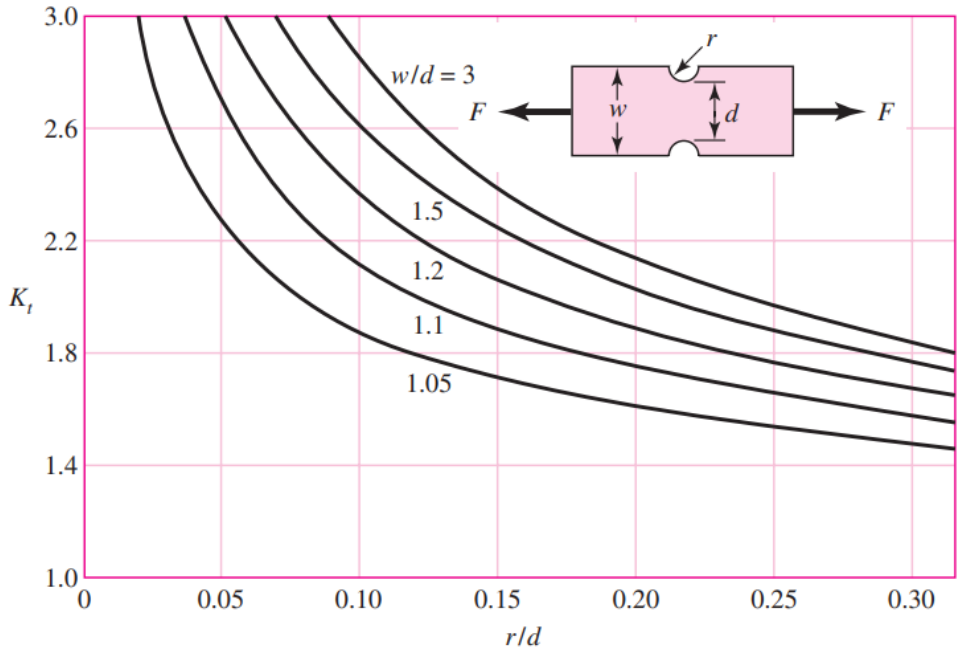


*Figure 3-11: Chart of Theoretical Stress-Concentration Factor $K_t$.*

For the sample used in this experiment, $r = 9.525\,mm$, $w = 88.9\,mm$, and $d = 44.45\,mm$. To determine the stress concentration factor $K_t$, ratio $r/d$ and $w/d$ are needed and which was 0.21 and 2 respectively. Since the value of $w/d = 2$ is not provided on the chart, the value of stress concentration factor was calculated as:

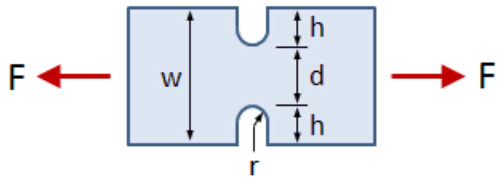


$$K_t = C_1 + C_2\left(\frac{2h}{w}\right) + C_3\left(\frac{2h}{w}\right)^2 + C_4\left(\frac{2h}{w}\right)^3 \qquad 3\text{-}1$$

Where the coefficients in the equation above are:

*Table 3-9: Coefficient for stress concentration factor. [34]*

| | **0.1 ≤ h/r ≤ 2.0** | **2.0 ≤ h/r ≤ 50.0** |
|---|---|---|
| $C_1$ | 0.955 + 2.169 √h/r − 0.081 (h/r) | 1.037 + 1.991 √h/r + 0.002 (h/r) |
| $C_2$ | −1.557 − 4.046 √h/r + 1.032 (h/r) | −1.886 − 2.181 √h/r − 0.048 (h/r) |
| $C_3$ | 4.013 + 0.424 √h/r − 0.748 (h/r) | 0.649 + 1.086 √h/r + 0.142 (h/r) |
| $C_4$ | −2.461 + 1.538 √h/r − 0.236 (h/r) | 1.218 − 0.922 √h/r − 0.086 (h/r) |

Using Equation 3-1 and Table 3-9, stress concentration factor was found to be 2.027. This stress concentration factor can be multiplied to nominal stress to find the actual stress.

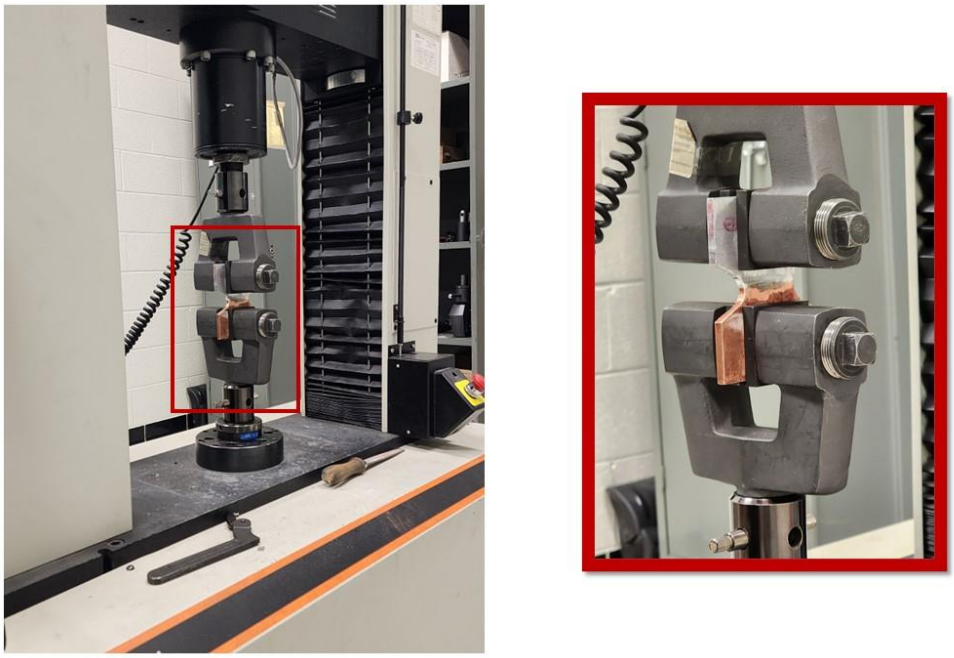

*Figure 3-12: Tensile test using Instron 5500R.*

Nominal stress is defined as force per unit area and can be calculated using Equation 3-2.

$$\sigma_0 = \frac{F}{A} \qquad 3\text{-}2$$

Where, $\sigma_0$ is nominal stress, $F$ is tensile load applied to the sample and $A$ is normalized cross-section area of the sample. Actual stress can be calculated as:

$$\sigma = \sigma_0 \times K_t \qquad 3\text{-}3$$

Strain is defined as a change in length per unit original length due to the load and can be calculated by using Equation 3-4.

$$\varepsilon = \frac{\Delta L}{L} \qquad 3\text{-}4$$

Where, $\varepsilon$ is strain, $\Delta L$ is change in length and $L$ is the original gauge length of the sample.

Sample after the tensile test was cut to see the fractured surface under the scanning electron microscope as shown in Figure 3-13.

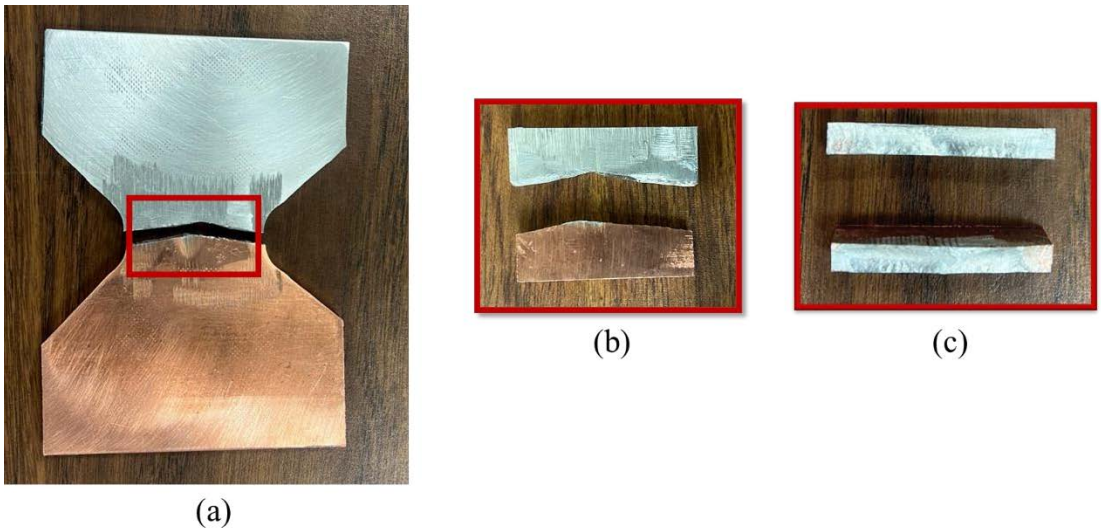


*Figure 3-13: Sample preparation for the microstructure analysis. (a) Sample fractured from tensile test. (b) Section of fractured part side view. (c) Section of fractured part top view.*

### 3.4.2 Nano indentation

Nanoindentation is a technique used to measure the mechanical properties of the material in very small scales, typically in nanometer range. It involves employing a sharp indentation, like diamond tip, to apply a controlled force to a material's surface, and measuring the resulting depth of the indentation. Properties like hardness, elastic modulus and viscoelastic behavior are identified by measuring the applied force and the resulting indentation. [13]

Hardness at the HAZs and junction was measured using nano indentation technique. The friction welded sample has very minimum, or no heat affected zone, so the hardness of the sample was on the parent material, junction and on parent material near to the welded junction. Nanovea nano indenter shown in Figure 3-14 was used for hardness measurement.

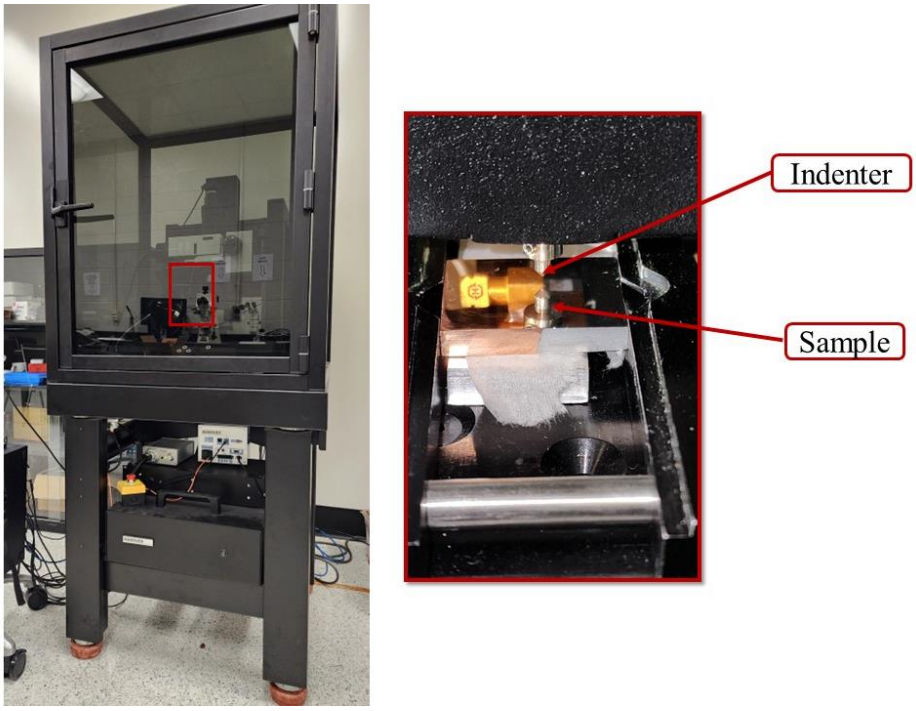


*Figure 3-14: Nanovea nanoindentation with test sample.*

Berkovich indentation was used for nano indentation. The Berkovich indenter has a pyramidal shape with a three-sided pyramid. Each face of the pyramid has an angle of 65.3 degree, resulting in a very sharp and pointed tip [14]. Figure 3-15 shows the schematic of Berkovich Indenter.

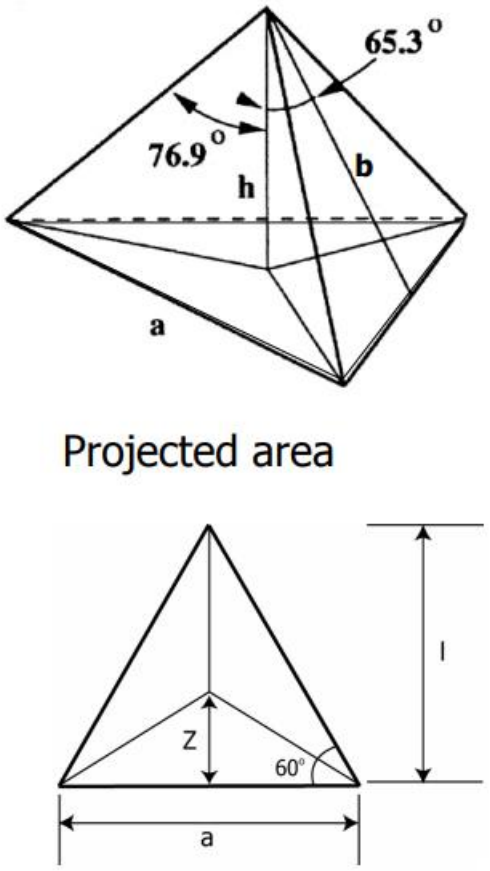


*Figure 3-15: Berkovich Indenter [15].*

Parameters used for nanoindentation analysis is shown in Table 3-10.

*Table 3-10: Parameters used for nanoindentation analysis.*

| Parameters | Value |
|---|---|
| **Approach Speed** | 10 $\mu m/min$ |
| **Contact Load** | 0.1 $mN$ |
| **Indenter** | Berkovich-Be 0070 |
| **Load** | 200 $mN$ |
| **Loading rate** | 100 $mN/min$ |
| **Unloading rate** | 100 $mN/min$ |

Figure 3-16 shows the schematic of loading and unloading curve obtained from the nano indenter.

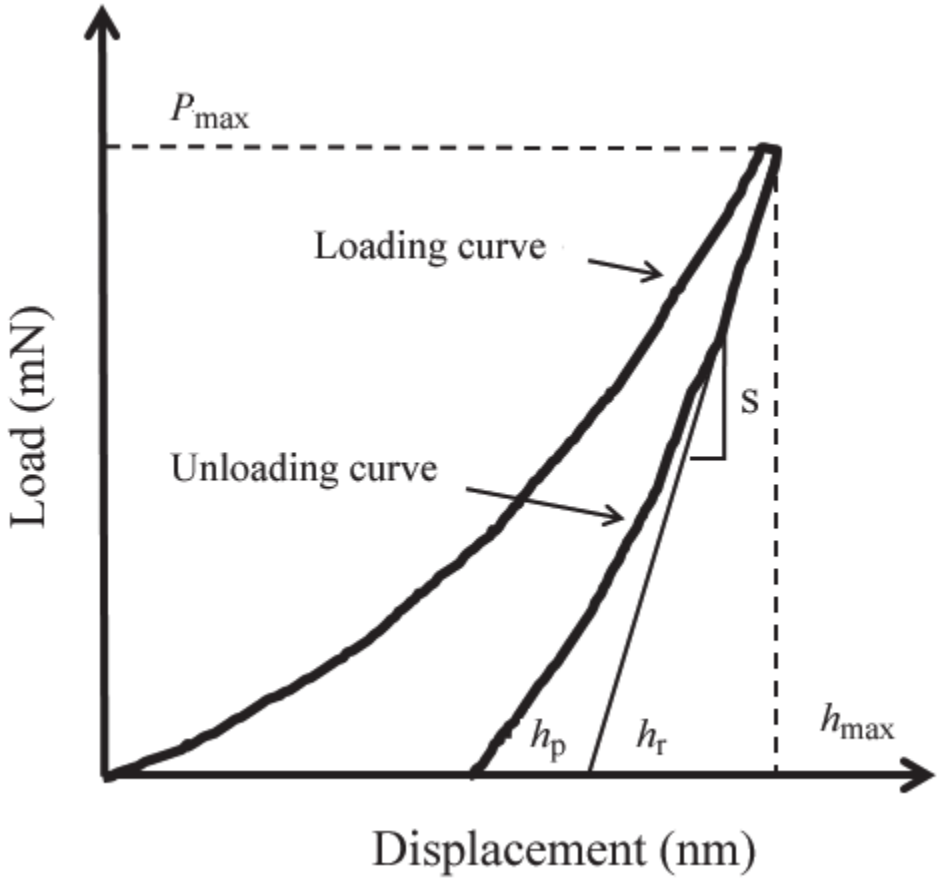


*Figure 3-16: Load and unloading curve [16].*

On the Figure 3-16, $P_{max}$ is the maximum load applied on the projected area $(A_{proj})$. Projected area for Berkovich indenter can be calculated as:

$$A_{proj} = 24.56h^2 \quad 3\text{-}5$$

Where $h$ is the penetration depth at maximum load.

Hardness can be calculated by using the Equation 3-6:

$$H = \frac{P_{max}}{A_{proj}} \quad 3\text{-}6$$

Hardness from Nanovea nanoindentation machine with Berkovich indenter gives the Berkovich hardness in GPa. Berkovich hardness (GPa) was converted to Vickers hardness (HV) to compare with other literature. Berkovich hardness (GPa) was converted to Vickers hardness (HV) using the Equation 3-7 below:

$$HV = \frac{GPa}{0.009807} \quad 3\text{-}7$$

### 3.4.3 Microstructure Analysis

Both welded sample fractured sample from tensile test was viewed under electron microscope. SEM and EDS analysis was done on the welded sample while only SEM was done on the fractured surface to see the type of fracture. SEM images give the understanding of the quality of weld at the welded region while the EDS will give the elemental composition at the different locations across the welded region. JEOL JIB-4500 shown in Figure 3-17 is used for SEM and EDS analysis. EDS analysis was done to see the effect of interlayer at the junction and

to see the difference in elemental composition with and without the interlayer. Elemental analysis can also provide the information about the formation of intermetallic compound at the interface. It is assumed that the formation of intermetallic compound is less in the sample with zinc interlayer.

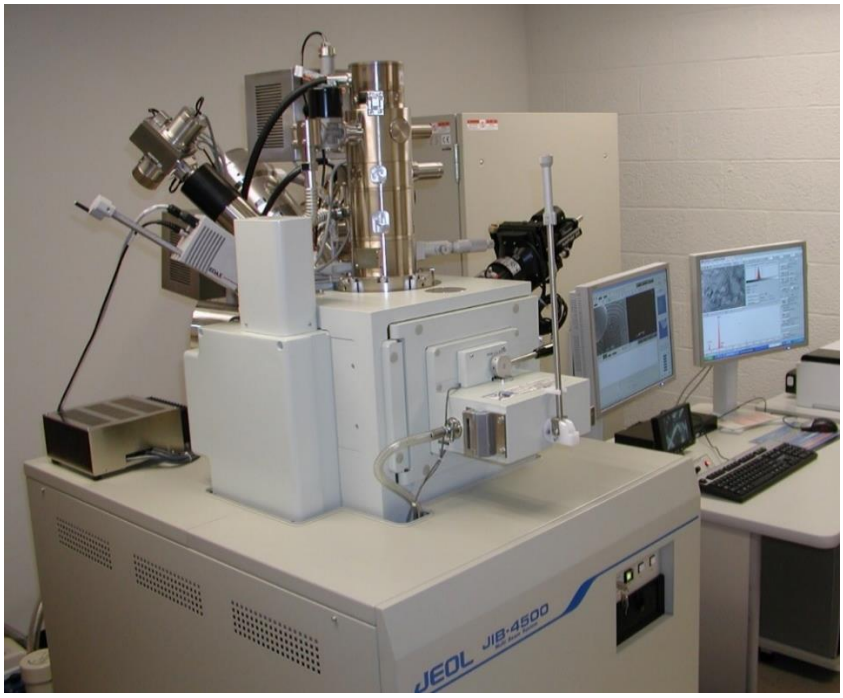


*Figure 3-17: JEOL JIB-4500 electron Microscope.*

### 3.4.4 Thermal Analysis

Junction temperature is a very important factor during friction welding. During friction welding, junction temperature should be below the melting point of parent materials. At the interface, heat is generated by direct conversion of mechanical energy into thermal energy [17]. There is the energy that is utilized during the oscillation to overcome the friction which is converted to thermal energy. Thermal energy at the interface raises the temperature at the

interface which is utilized for welding. The main objective of this analysis was to find the right parameters like amplitude and frequency that can produce the desirable temperature at the interface. Temperature at the interface should not exceed the melting point of the parent material. For this analysis, temperature across the junction was measured using the FLIR Infrared (IR) camera for certain parameters. Using those parameters as a boundary condition, numerical analysis was done to see if the analytical temperature profile matches the experimental temperature profile. For this analysis following assumptions were made:

a) Friction from the bearings supporting the tooling is negligible.

b) Movement of the samples in the tooling is minimal.

c) Energy going into the specimen from the burn-off can be ignored.

Figure 3-18 shows the schematic of the Linear friction welder. On the Figure $F_{Total}$ is the total force provided by the machine, $F_{int}$ is the force at the interface to overcome the friction and $F_{oss}$ is the total force required to oscillate the machine.

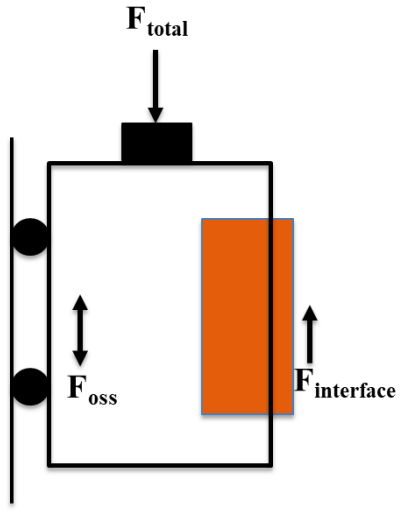


*Figure 3-18: Schematic of Linear Friction Welding.*

Position of oscillator $(x)$ during the welding can be calculated as:

$$x = Asin(2\pi ft) \tag{3-8}$$

Position was integrated w.r.t time to get the velocity at the specific location.

$$v = \frac{dx}{dt} = A2\pi f(2\pi ft) \tag{3-9}$$

Using central finite difference approximation velocity and the acceleration at an instant can be calculated using:

$$v_i = \frac{1}{2dt}(-x_{i-1} + x_{i+1}) \tag{3-10}$$

$$a_i = \left(\frac{x_{i+1} + 2x_i + x_{i-1}}{dt^2}\right) \tag{3-11}$$

On the Equation 3-10 and 3-11 above $x_i$ is the position of the oscillator at time $t$, $x_{i-1}$ is the position of the oscillator at time $t - dt$ and $x_{i+1}$ is the position of the oscillator at time $t + dt$. Figure 3-19 shows the schematic of the position and time of the oscillator.

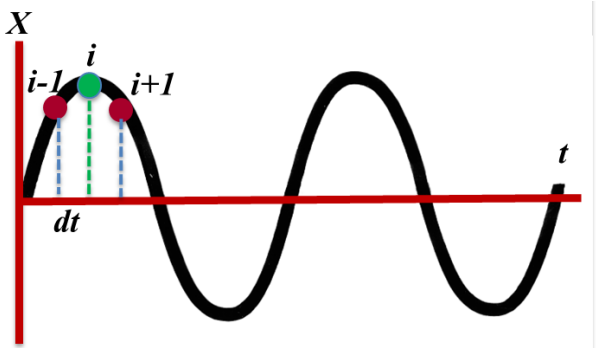


*Figure 3-19: Schematic of position and time of the oscillator.*

Total force required for the welding was obtained from the friction welding machine. Force obtained from the machine was used to oscillate the system and to overcome the friction. One the mass and the acceleration of the system is known, total force required to oscillate was known by using Equation 3-12:

$$F_{oss} = M \times a \tag{3-12}$$

Here M is the mass of the oscillator, and the a is the acceleration of oscillator obtained from Equation 3-11.

Once the $F_{oss}$ is known, force required to overcome the friction can be calculated using Equation 3-13.

$$F_{int} = F_{Total} - F_{oss} \tag{3-13}$$

During friction welding, temperature rise occurs primarily due to the conversion of mechanical energy into heat energy at the weld interface which is known as frictional heating. The heat generated through friction causes the localized temperature to rise significantly, facilitating the welding process [25]. Energy at the interface can be calculated using Equation 3-14 below:

$$E_{int} = \int_0^T F_{int} v \, dt \tag{3-14}$$

Here $E_{int}$ is the mechanical energy which is converted to heat energy to raise the temperature at the interface. For the thermal analysis $E_{int}$ was used as an energy source for the temperature rise. There is loss of energy at the same time due to the conduction, convection, and

radiation from the junction. Figure 3-20 shows the schematic of the heat transfer from the specimen during the friction welding process.

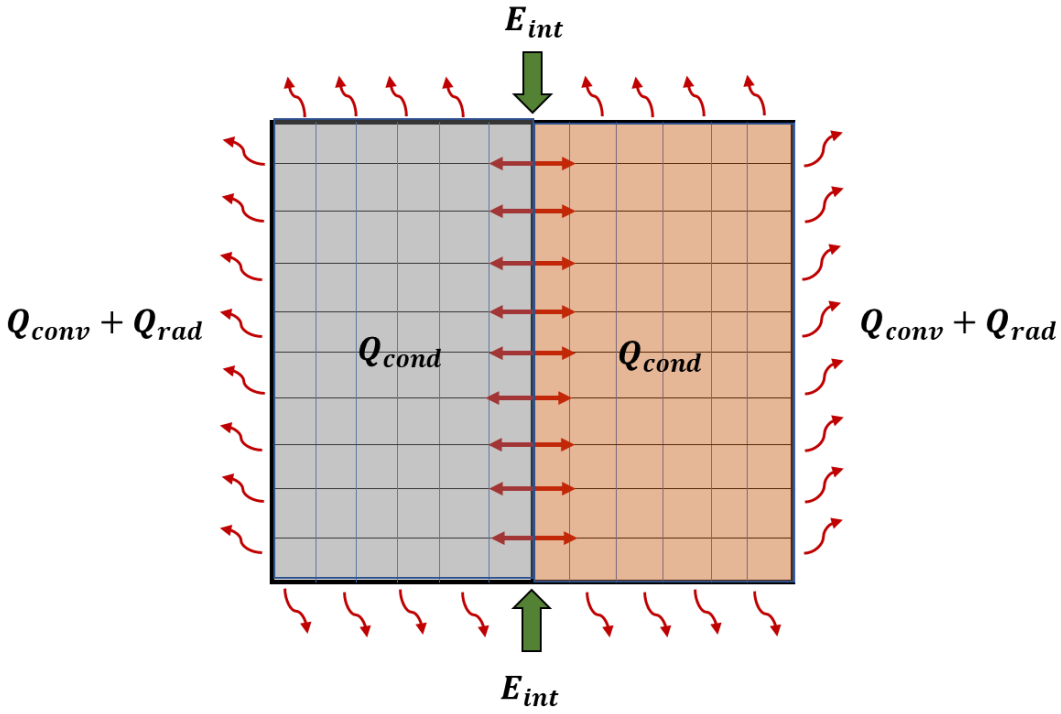


*Figure 3-20: Schematic of heat transfer from the specimen during friction welding.*

At the interface, boundary conditions with combined convection and radiation are given by:

$$hA(T_\infty - T_{int}) + \varepsilon\sigma A\left(T_{surr}^4 - T_{int}^4\right) + kA\frac{T_1 - T_{int}}{\Delta x} + E_{int} = 0 \qquad 3\text{-}15$$

Where $h$ is heat transfer coefficient, $T_\infty$ is the ambient temperature, ε is the emissivity, σ is Stefan-Boltzmann constant, $T_{surr}$ is the surrounding temperature, $T_{int}$ is the temperature at the interface, $k$ is the thermal conductivity of the material and $T_1$ is the temperature at the next node from the interface.

Heat transfer coefficient depends on the various properties of the air such as Specific heat capacity, thermal conductivity, thermal diffusivity, dynamic viscosity, kinematic viscosity, and Prandtl number. Convection during the friction welding process is natural convection and the specimen is vertical plate. Nusselt number for natural convection over the flat plate is given by:

$$Nu = \left[0.825 + \frac{0.387 Ra_L^{1/6}}{[1 + (0.492/Pr)^{9/16}]^{8/27}}\right]^2 \quad \text{3-16}$$

Where $Ra_L$ is the Rayleigh number, which is the product of the Grashof number, which describes the relationship between buoyancy and viscosity within the fluid, and Prandtl number, which describes the relationship between momentum diffusivity and thermal diffusivity. Rayleigh number can be calculated as:

$$Ra_L = Gr_L Pr = \frac{g\beta(T_s - T_\infty)L_c^3}{\mu^2} Pr \quad \text{3-17}$$

Once the Nusselt number is known, heat transfer coefficient can be found using:

$$h = \frac{Nu \times k}{L_c} \quad \text{3-18}$$

Where, $k$ is the thermal conductivity of the air and $L_c$ is the characteristic length of the specimen.

Those properties of the air depend on the temperature and changes with change in temperature. To know the trendline of the change of properties, change in properties was plotted on excel and the equation was determined. Figure 3-21 shows the change in properties of air with temperature and Figure 3-22 shows the change in heat transfer coefficient with change in temperature.

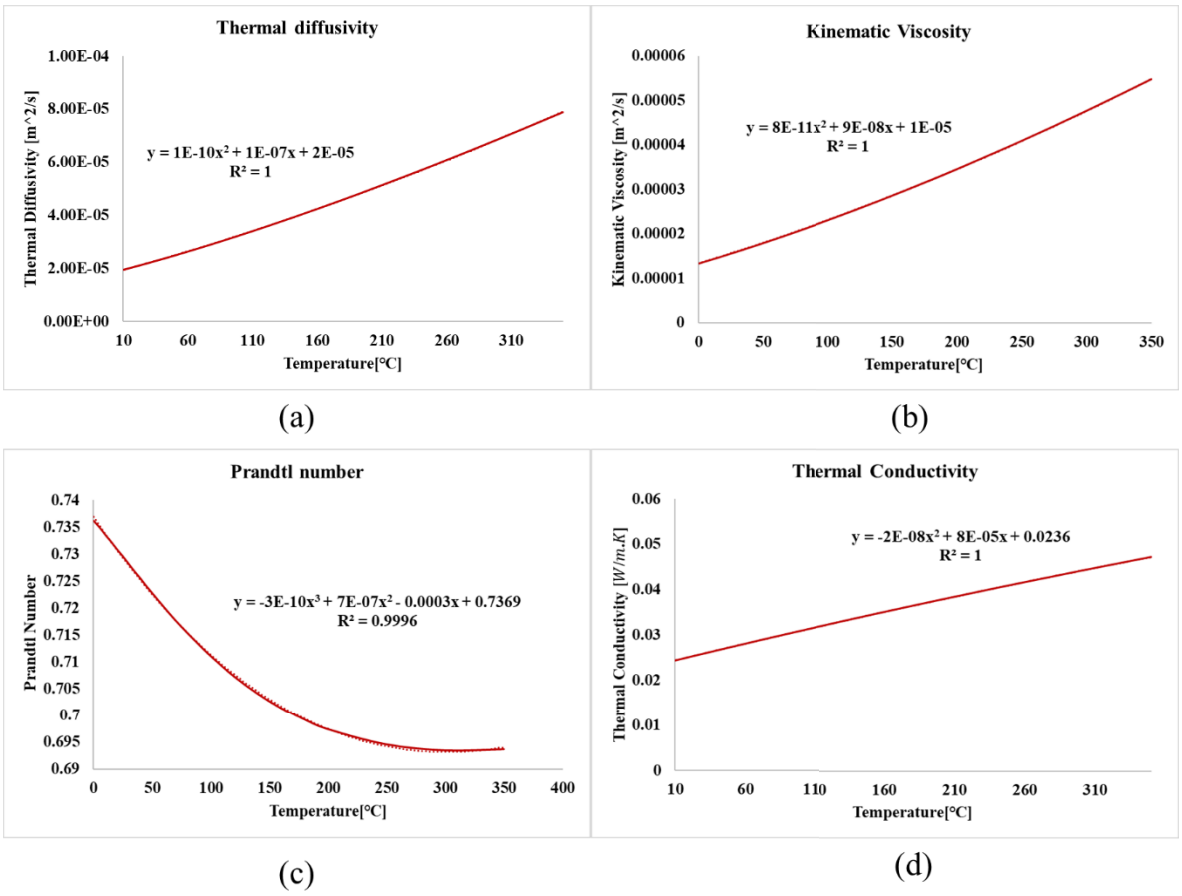


*Figure 3-21: Change is air properties with temperature. (a) Thermal diffusivity, (b) Kinematic Viscosity, (c) Prandtl number, (d) Thermal Conductivity*

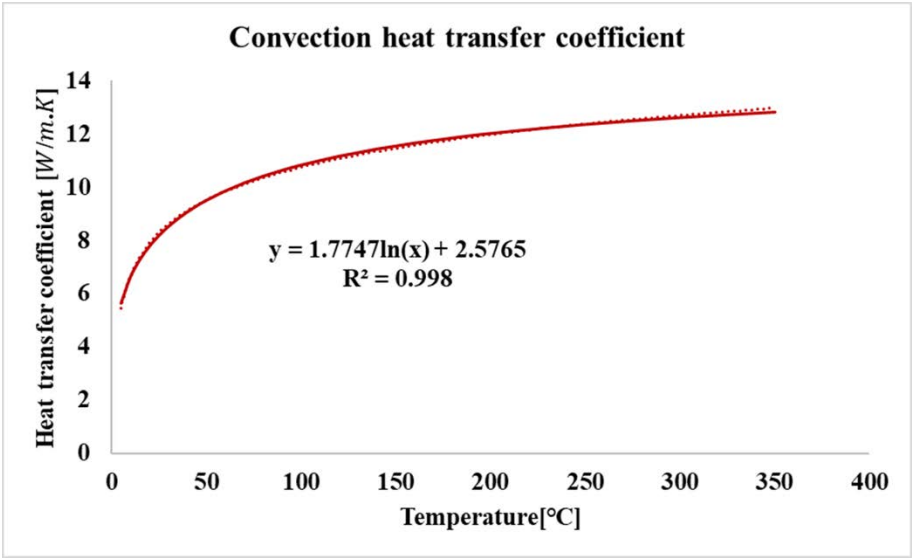


*Figure 3-22: Change in convection heat transfer coefficient with change in temperature.*

For thermal analysis, MATLAB code was used. Plot fitted equations shown in Figure 3-21 and 3-22 was used in MATLAB to incorporate the variable properties of air with temperature. Similarly, the emissivity value of copper and aluminum also changes with the change in temperature. Change in emissivity for both copper and aluminum were obtained from literature review.

Heat transfer during the friction welding is transient heat transfer, which means the temperature changes with time as well as position. The finite difference formulation of time-dependent problems involves discrete points in time as well as space as shown in Figure 3-23.

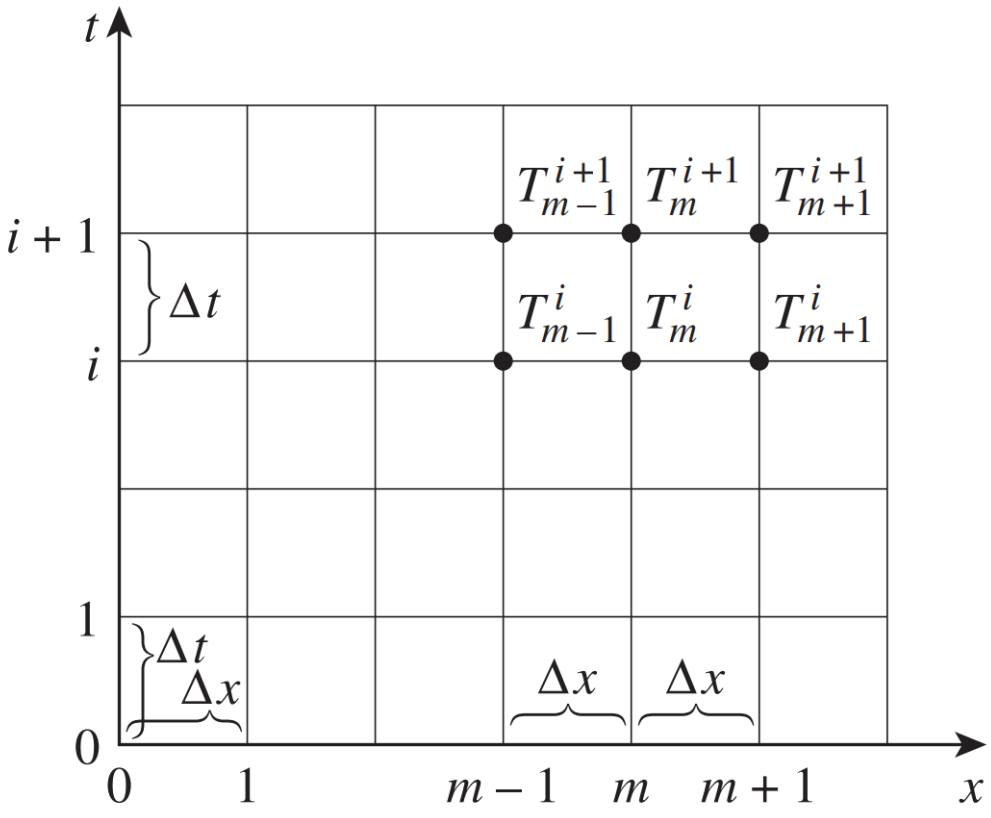


*Figure 3-23: Discrete points in time as well as space [27].*

For the transient heat transfer, nodes and the volume elements are selected as they are in steady state case. The energy balance on a volume element during a time interval $\Delta t$ can be expressed as:

$$\Delta t \times \sum_{All\ Sides} \dot{Q} + \Delta t \times \dot{E_{gen,element}} = \Delta E_{element} \quad 3\text{-}19$$

Where rate of heat transfer $\dot{Q}$ consist of conduction, convection, and radiation. And the term $\Delta E_{element} = mc_p \Delta T$.

Implicit finite difference formulation for the transient heat transfer involving conduction, convection and radiation can be expressed as:

$$T_{m-1}^{i+1} = \left(1 - 2\tau - 2\tau\frac{h_{comb}\Delta x}{k}\right) T_{m-1}^{i} + 2\tau T_m^i + 2\tau\frac{h_{comb}\Delta x}{k} T_\infty + \tau\frac{\dot{E_{m-1}^{\iota}}\Delta x^2}{k} \quad 3\text{-}20$$

Here, $h_{comb}$ is the combined heat transfer coefficient for convection and radiation which is given by:

$$h_{comb} = h_{conv} + h_{rad} = h_{conv} + \varepsilon\sigma(T_s + T_{surr})(T_s^2 + T_{surr}^2) \quad 3\text{-}20$$

$\tau$ is the dimensionless mesh Fourier number which is defined as:

$$\tau = \frac{\alpha\Delta t}{\Delta x^2} \quad 3\text{-}21$$

Where $\alpha = k/\rho c_p$ is the thermal diffusivity of the material.

Equation 3-20 was used in MATLAB to analytically find the temperature distribution on the sample and the temperature distribution was compared with the experimental temperature obtained from IR camera shown in Figure 3-24.


*Figure 3-24: IR camera used during experiment.*

# 4 Results and Discussion

## 4.1 Comparison of Welds with and without Interlayer

The welded samples were examined to see if there are any cracks present in the welding region. It was found that there were no visible cracks present on either of the sample with or without the interlayer. Specimen was viewed under digital microscope to see for the cracks. Figure 4-1 shows the welding without the interlayer in different magnification and Figure 4-2 shows the welding with interlayer.

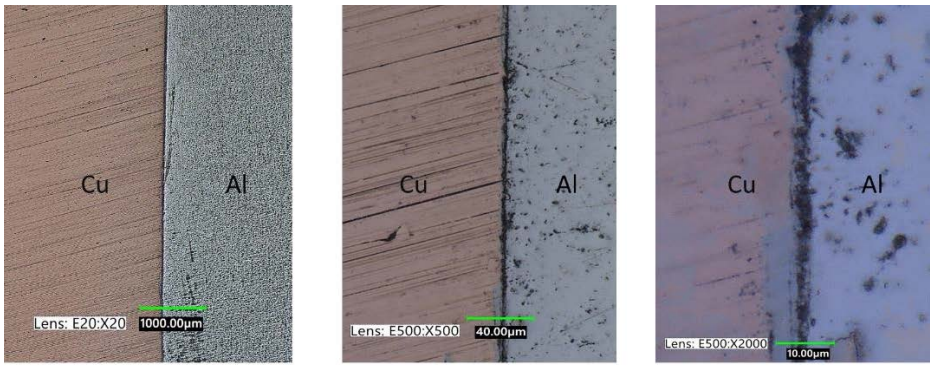


*Figure 4-1:Welding without interlayer viewed under digital microscope, (a) ×20, (b) ×500, (c) ×1000.*

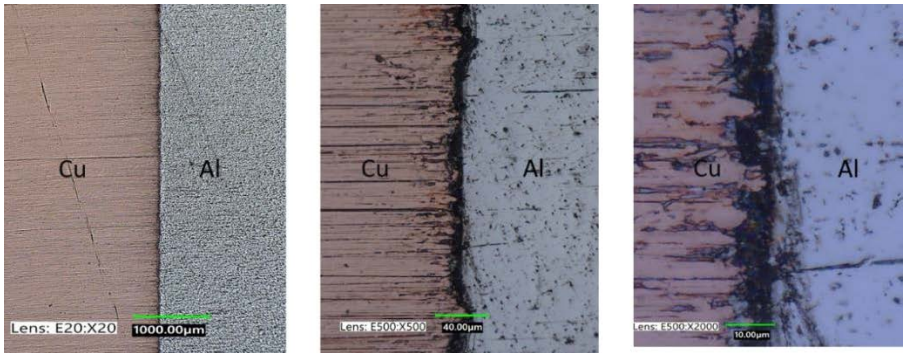


*Figure 4-2: Welding with interlayer (200µm) viewed under digital microscope. (a) ×20, (b) ×500, (c) ×1000.*

Zinc has the melting point of $420\ °C$, but the temperature during the friction welding reach above $600\ °C$. So, the zinc interlayer is melted during the friction welding and formed a compound with copper and aluminum. Figure 4-2 viewed under digital microscope shows the burnt compound at the junction of Cu and Al, that is due to the zinc melting during the welding. While there was no distinction between two welded samples with naked eye, difference can be seen when we magnify the welded junction.

## 4.2 Microstructure Analysis

Both samples with and without interlayer were viewed under electron microscope. It was found that welding without the interlayer has multiple cracks along the weld line. This is primarily due to the formation of brittle intermetallic compounds like $Cu_2Al$, $Cu_3Al_2$, $Cu_4Al_3$ etc. Copper and Aluminum have high chemical affinity for each other so there is formation of such intermetallic compounds. Although the amount of those intermetallic compounds is significantly lower than the traditional fusion welding, those brittle compounds are still present during the friction welding process [26]. Figure 4-3 shows the cracks present in the welded junction of copper and aluminum. Most cracks were seen on the copper side of the welded sample. Such cracks were present on all the sample that were welded without the interlayer. Figure 4-4 shows the SEM image of the welded junction with interlayer. There were no cracks present on the sample that was welded with Zinc interlayer. Thickness of zinc interlayer was $200\ \mu m$ but majority of the zinc was melted and squeezed during the welding process so only about $10\ \mu m$ thickness of zinc interlayer was present on the welded sample.

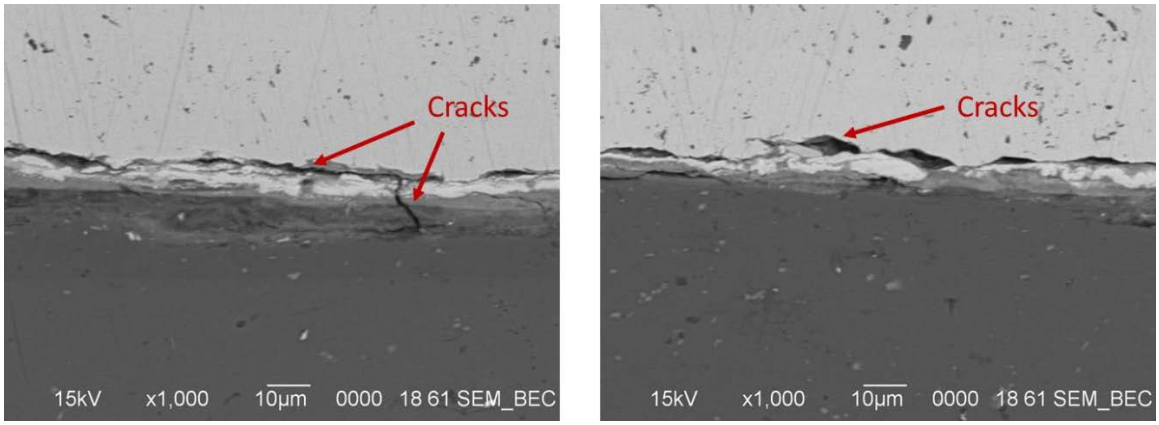


*Figure 4-3: SEM image of the welded junction without interlayer.*

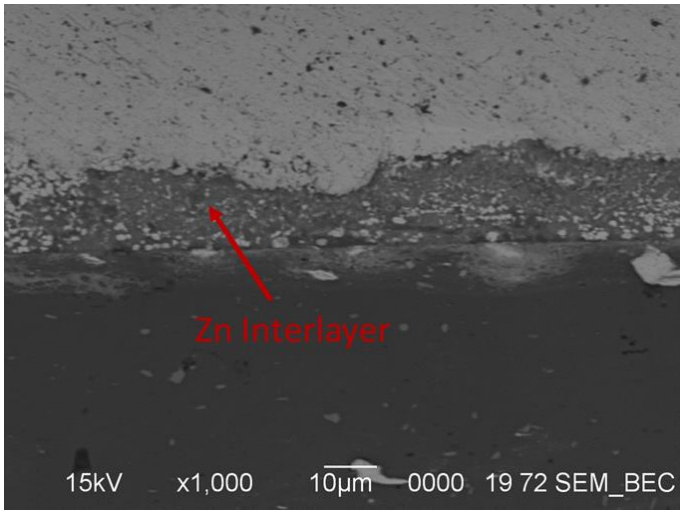


*Figure 4-4: SEM image of the welded junction with interlayer (200µm).*

When multiple SEM images are analyzed, it was found that there was no heat affected zone present on the sample. This is because of the production of the flash during the friction welding. All the materials which are affected by the heat are removed from the actual welded junction due to the immense forging pressure during the welding. It was also found that on some samples which were welded with the interlayer material, there is no sign of interlayer material seen while viewing under the electron microscope. This might be because of the melting and

squeezing of the zinc interlayer during the welding process. It was also found the welding junction was not straight for all the samples. This might be because of uneven temperature and pressure distribution at the junction during the welding. Uneven temperature might be due to the impurities present on the sample.

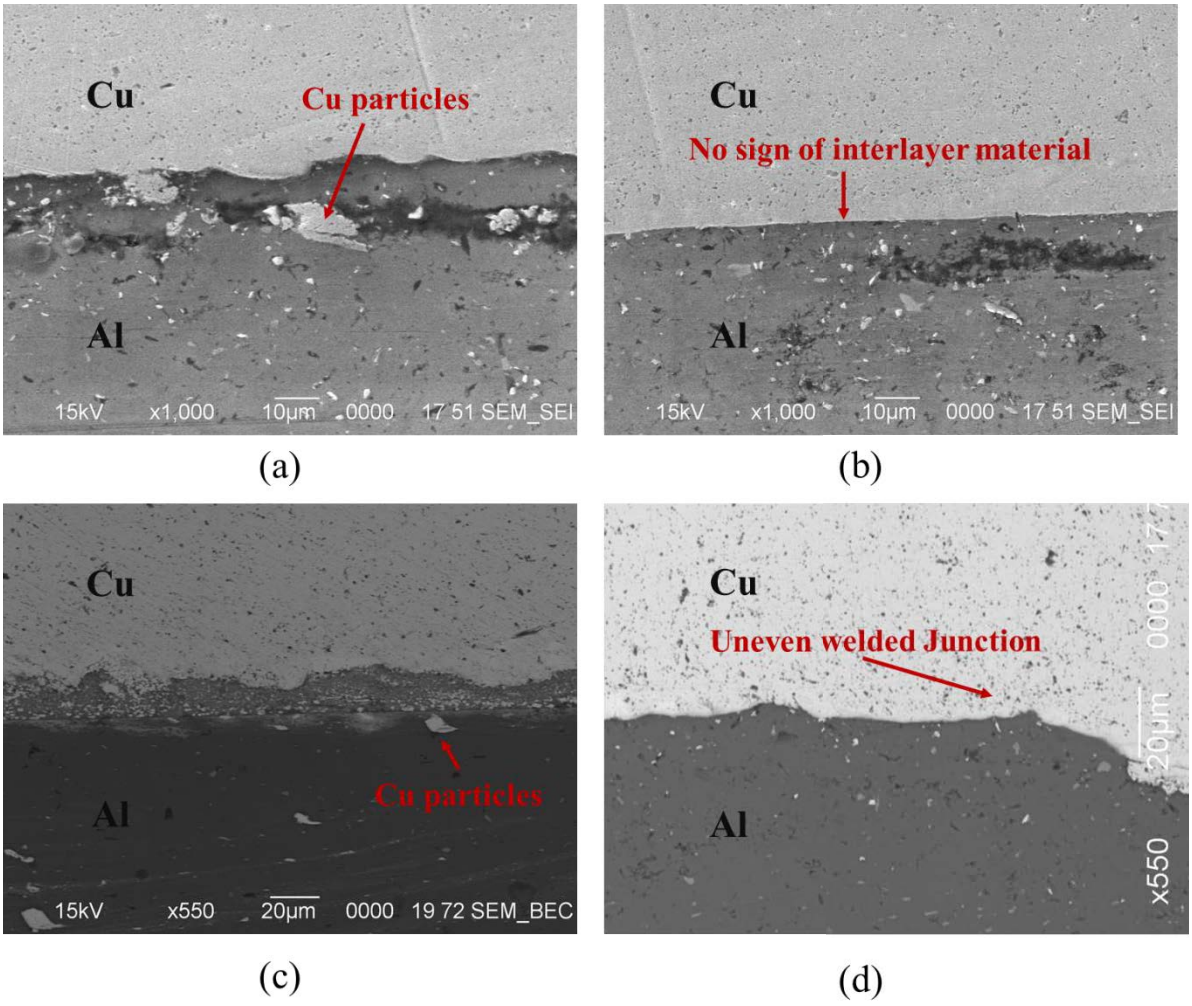


*Figure 4-5: Different features in welded junction (a )welding with* 200 *µm interlayer* × 1000 *, (b) welding with* 70 *µm interlayer* × 1000*, (c) welding with* 200 *µm interlayer* × 550*, (d) welding without interlayer* × 550.

The fractured surface of the sample after the tensile test were viewed under microscope to see the mode of fracture. Both samples with and without interlayer were viewed under the SEM.

Fractography plays an important role in determining the mode of failure by proving visual evidence and characteristic features associated with different failure modes. Features such as crack propagation, microvoid coalescence, deformation bands, and fatigue striations can be observed under the microscope which will determine the mode of failure [28]. Figure 4-6 shows the fractures surface of aluminum and copper welded with the interlayer and Figure 4-7 shows the fracture surface of aluminum and copper welded without the interlayer.

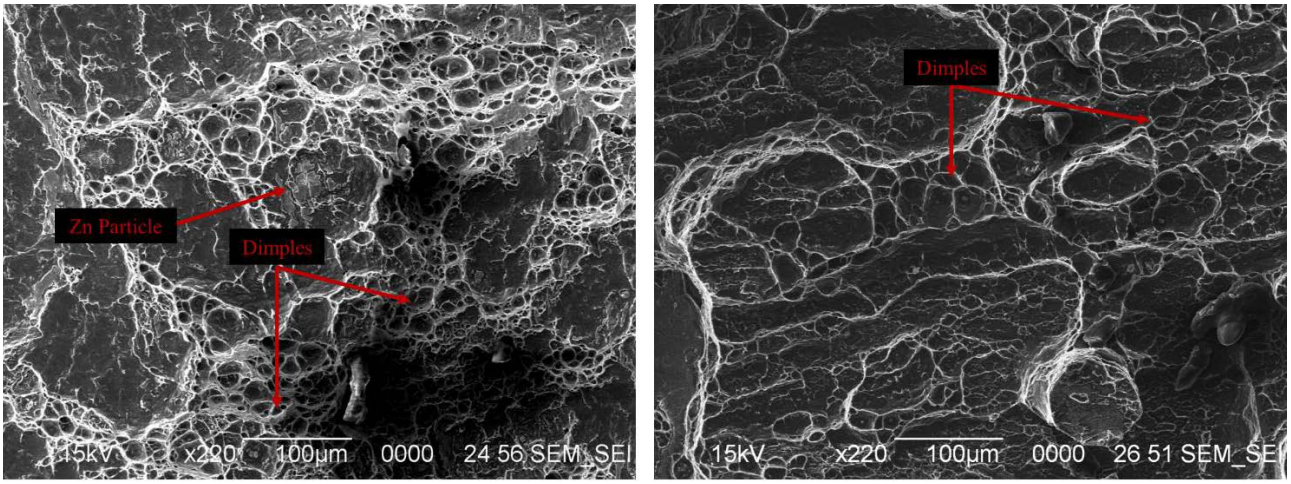


*Figure 4-6: SEM image of fractured surface of (a) Aluminum and (b) Copper welded with Zn interlayer.*

As seen in Figure 4-6 there are features such as microvoid coalescence and Cleavage present on the fractured surface. Microvoid coalescence is characteristic of ductile fracture. During yielding, as the metal stretches voids are formed around tiny inclusions in the metal. Those small voids eventually combine to create larger voids and, eventually, fracture [29]. Cleavage on the other hand is the characteristic of the brittle fracture. There are some portions on the SEM image where there is no microvoid coalescence but cleavage. This suggests that the welding is not perfectly ductile, and the welding is not uniform. It was also seen that the

aluminum side has more dimple structures than the copper side. There were also traces of zinc which were stuck on either side of the junction.

Figure 4-7 have features such as cleavage and dendritic structure. Microvoid coalescence were not seen in the SEM images of the welding without the interlayer. One of the interesting findings in the image is that there is presence of copper particle on the aluminum side and presence of aluminum on the copper side. There is a river pattern in the fractured surface suggesting it is a brittle fracture. On the copper side, there is the presence of small rounded dendritic structures. The rounded dendritic structures on the fracture are the result of melting during the friction welding process. This results in a brittle, low-strength structure [30].

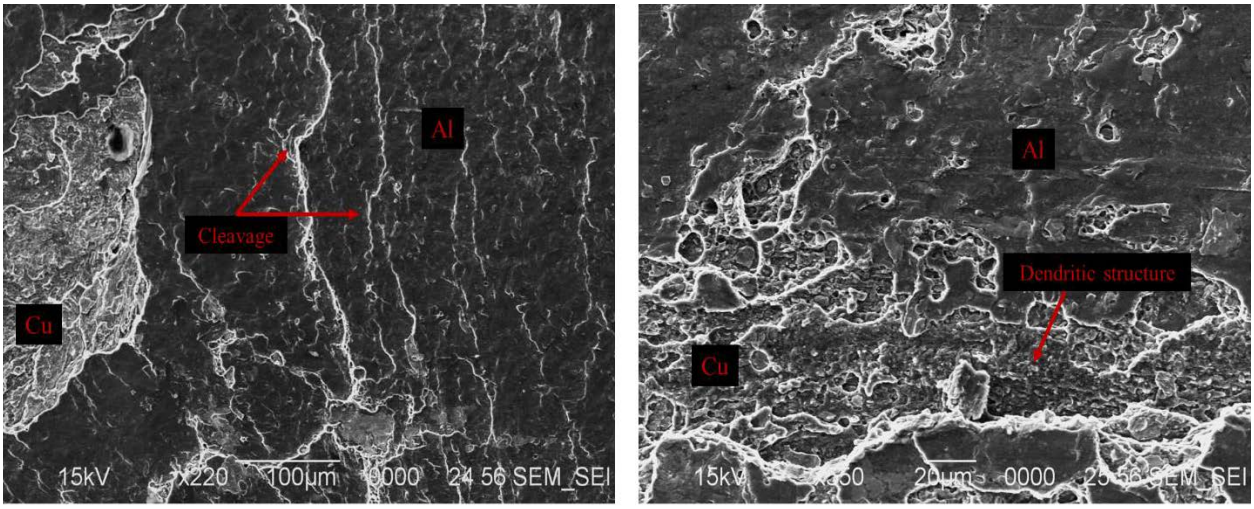


**(a)** **(b)**

*Figure 4-7:SEM image of fractured surface of (a) Aluminum and (b) Copper welded without interlayer.*

EDS analysis was done to determine the elemental compositions across the weld regions, Figure 4-8 shows the compositional area mapping of the welded junction without interlayer. There is formation of oxides at the interface of copper and aluminum. There are also traces of

both aluminum and copper at the interface suggesting the formation of Cu-Al intermetallic compound at the interface. There was also the presence of carbon at the junction which are due to the impurities on the sample which are burnt to form a carbon and while handling the sample.

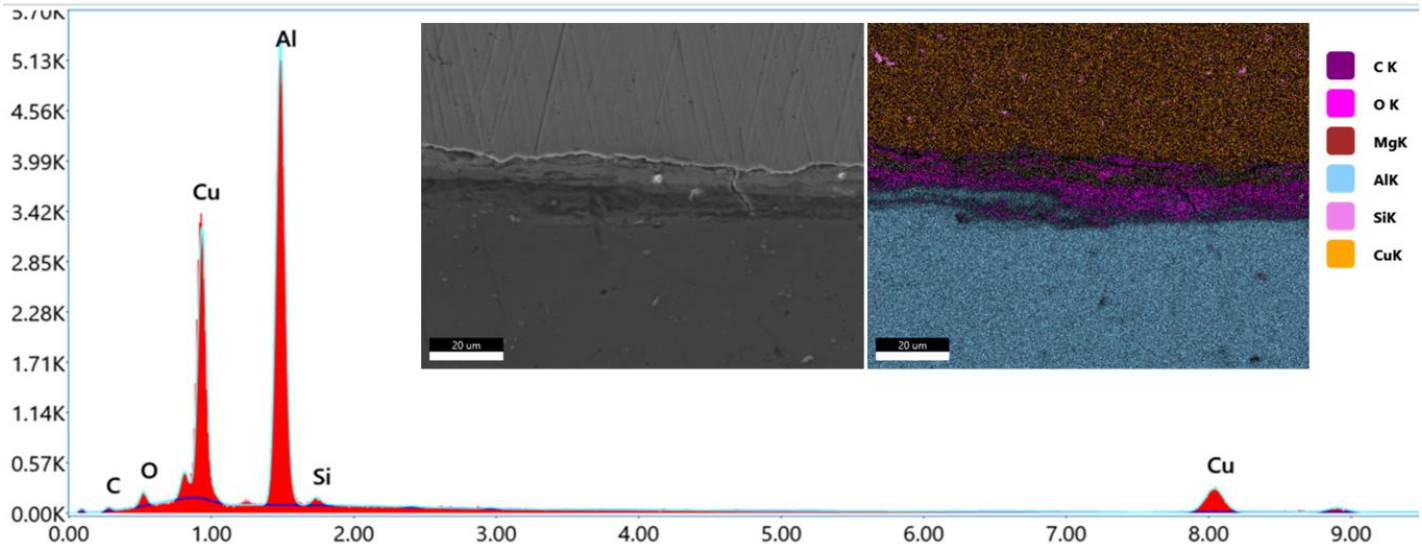


*Figure 4-8: Area mapping EDS analysis of the weld without interlayer.*

Table 4-1 shows the composition of the element on the sample. Significant number of oxides was seen at the junction which made it brittle. Formation of oxides can be inhibited by introduction of inert gas like argon during welding.

*Table 4-1: Elemental analysis on the weld without interlayer*

| **Without Interlayer-Analysis Uncertainty 9.55%** | | |
|---|---|---|
| **Element** | **Wt. %** | **Atomic %** |
| **Al** | 46.5 | 53.58 |
| **Cu** | 42.3 | 20.69 |
| **O** | 6.17 | 11.22 |
| **C** | 7.47 | 19.34 |
| **Si** | 1.02 | 1.13 |

Figure 4-9 shows the compositional area mapping of the welded junction with Zn interlayer. There is layer of Zn present on the junction as seen in figure. There is formation of oxides at the junction, however, concentration of oxides is less than the junction without the interlayer. It is seen that the oxides are formed only on the aluminum side, this might be because the aluminum has higher oxidation values than copper. Moreover, zinc has higher affinity with oxygen than copper, so there is formation of zinc oxides which inhibit the formation of oxides on copper side.

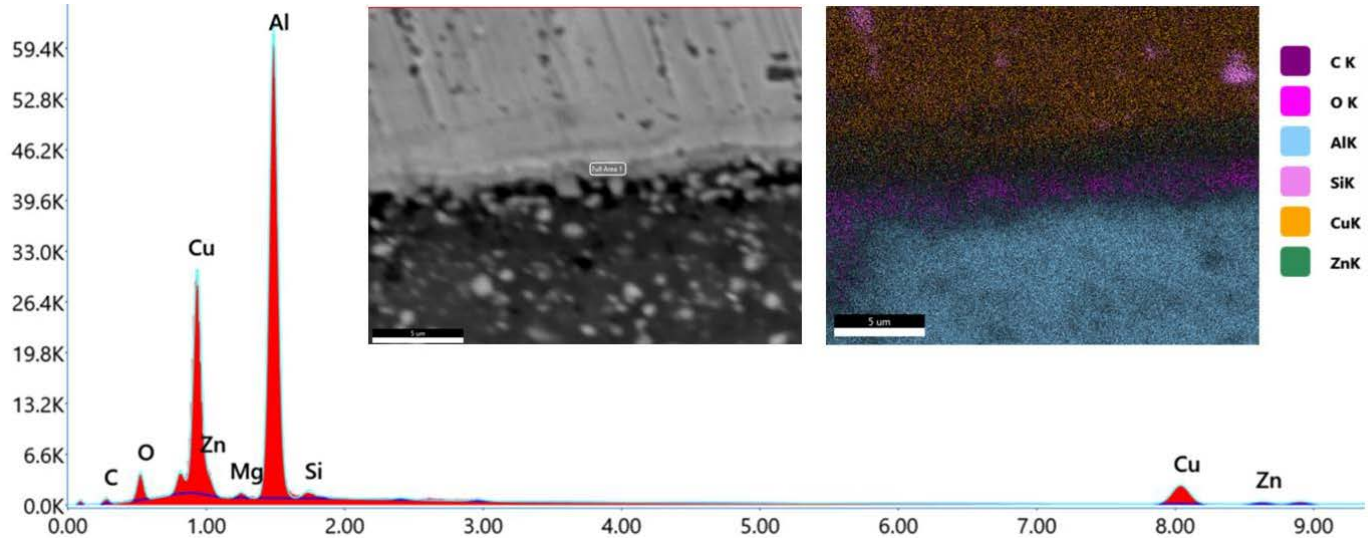


*Figure 4-9:Area mapping EDS analysis of the weld with interlayer* $(200\mu m)$

Table 4-2 shows the composition of the sample with zinc interlayer. There was formation of oxides with the zinc interlayer as well. Zinc interlayer inhibits the formation of intermetallic compounds but to avoid the formation of oxides, inert gas like Argon should be introduced during welding.

*Table 4-2:Elemental analysis on the weld with interlayer* $(200\mu m)$

| With Interlayer-Analysis Uncertainty 7.28% | | |
|---|---|---|
| **Element** | **Wt. %** | **Atomic %** |
| **Al** | 44.67 | 47.66 |
| **Cu** | 32.5 | 14.72 |
| **O** | 5.21 | 9.37 |
| **Zn** | 6.13 | 2.7 |
| **C** | 5.97 | 23.9 |
| **Si** | 0.95 | 0.97 |

## 4.3 Mechanical Properties Analysis

### 4.3.1 Tensile test

#### *4.3.1.1 Tensile test for sample without interlayer*

Welded sample without the interlayer was introduced for the tensile test to determine the strength of the weld. The maximum tensile strength of the welded sample ranges from 136 MPa to 154 MPa and the elongation ranged from 0.032 to 0.041. The difference in maximum tensile strength is due to different burn off distances that were achieved during the welding. The tensile strength of the welded junction is directly related to the burn off distance while welding the sample. Figure 4-5 shows the stress and strain curve for various samples welded without the interlayer.

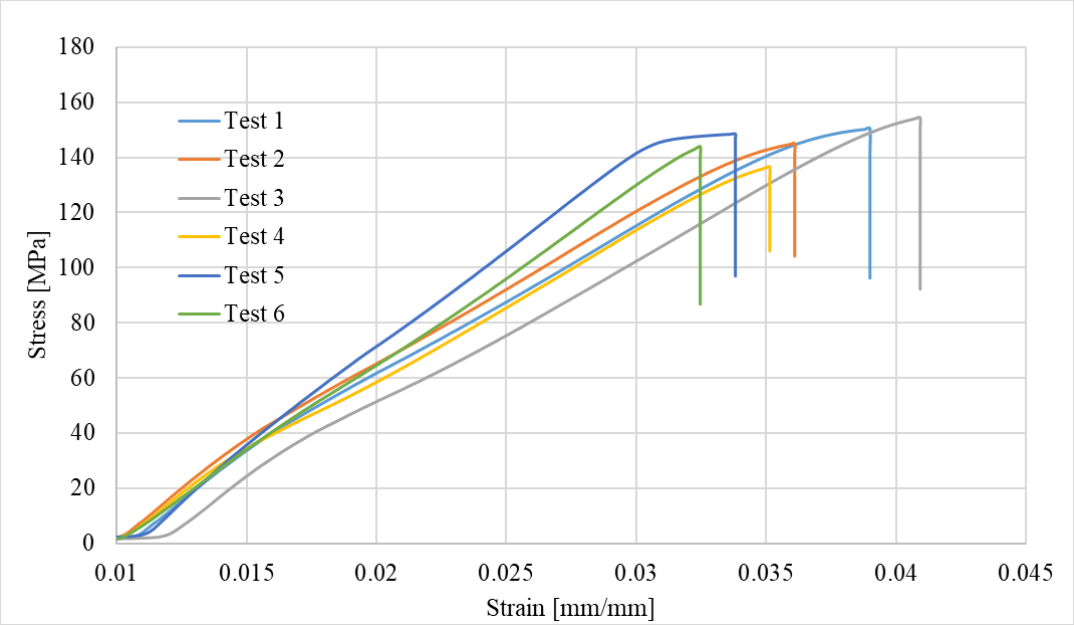


*Figure 4-10: Tensile test of welded sample without interlayer.*

Table 4-1 shows the maximum tensile strength for various samples and Figure 4-6 illustrate the results in line graph diagram.

*Table 4-3: Maximum Tensile strength of sample without interlayer.*

| **Without interlayer** | | |
|---|---|---|
| **Samples** | **Stress [MPa]** | **Strain (%)** |
| **1** | 150.58 | 3.89 |
| **2** | 144.995 | 3.61 |
| **3** | 154.303 | 4.09 |
| **4** | 136.417 | 3.51 |
| **5** | 148.538 | 3.38 |
| **6** | 143.995 | 3.25 |
| **Average** | **146.47** | **3.62** |
| **SD** | **11.31** | **0.29** |

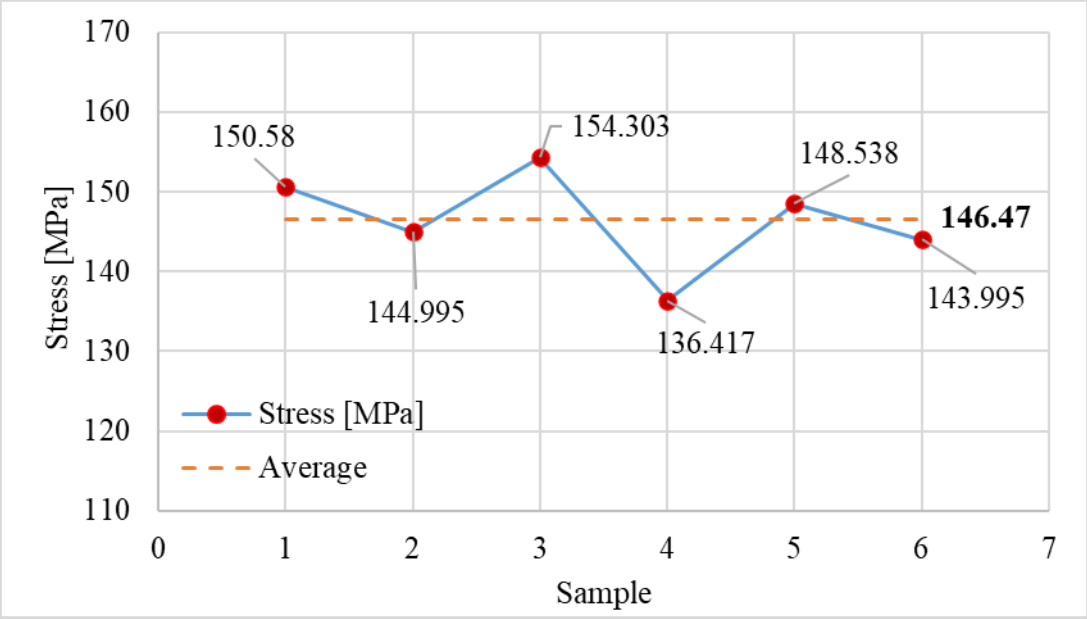


*Figure 4-11: Maximum tensile strength of sample without interlayer.*

Average tensile strength of the sample without the interlayer was found to be 146.47 MPa with the standard deviation of 11.31 and the average strain was 0.036 with the standard deviation of 0.29. The nature of the fracture was brittle fracture which can be explained by the SEM image of the fractured surface. The difference in maximum tensile strength is due to various reasons while performing the LFW. One of the main reasons was the burn off distance. Samples with higher burn off distance have slightly higher maximum tensile strength but to verify these results more samples were needed.

#### *4.3.1.2 Tensile test for sample with interlayer (0.07mm and 0.2mm)*

Welded samples with two different thicknesses zinc interlayers of 0.07mm and 0.2mm were introduced to the tensile test. For the welded sample with 0.2mm the maximum tensile strength ranges from 174.01 MPa to 197.41 MPa with the average tensile strength of 187.58 MPa

with standard deviation of 16.15. Figure 4-7 shows the stress strain curve for the welded sample with 0.2 mm Zn interlayer.

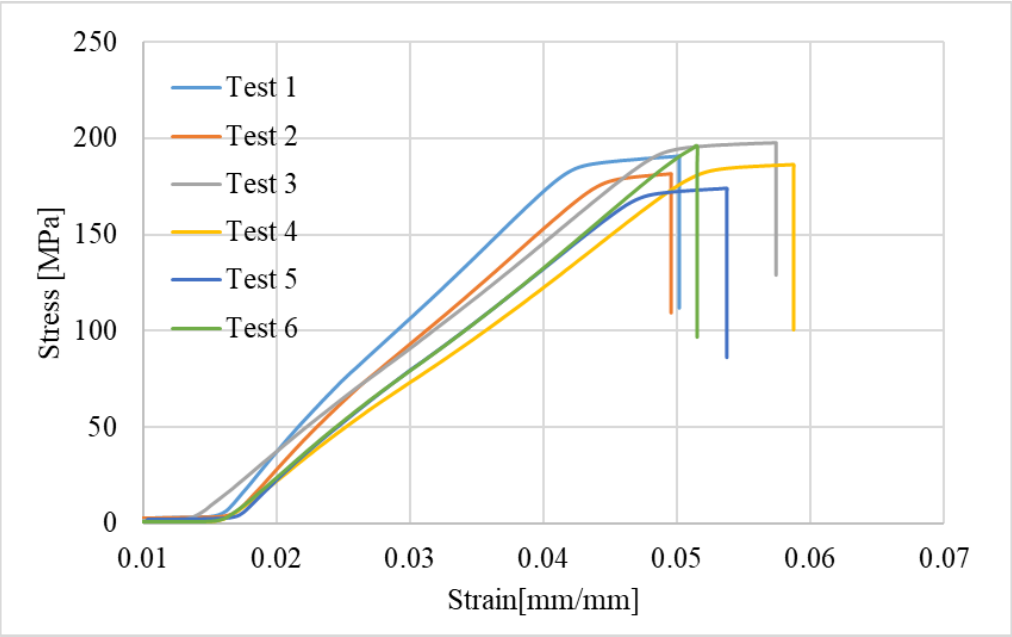


*Figure 4-12: Tensile test of welded sample with 0.2mm Zn interlayer.*

Table 4-4 shows the maximum tensile strength for various samples and Figure 4-8 illustrate the results in line graph diagram.

*Table 4-4:Maximum Tensile strength of sample with 0.2 mm interlayer.*

| **With interlayer 0.2 mm** | | |
|---|---|---|
| **Samples** | **Stress [MPa]** | **Strain (%)** |
| **1** | 190.62 | 5.19 |
| **2** | 181.74 | 4.96 |
| **3** | 197.41 | 5.74 |
| **4** | 186.06 | 5.87 |
| **5** | 195.64 | 5.15 |
| **6** | 174.01 | 5.37 |
| **Average** | **187.58** | **5.38** |
| **SD** | **16.15** | **0.33** |

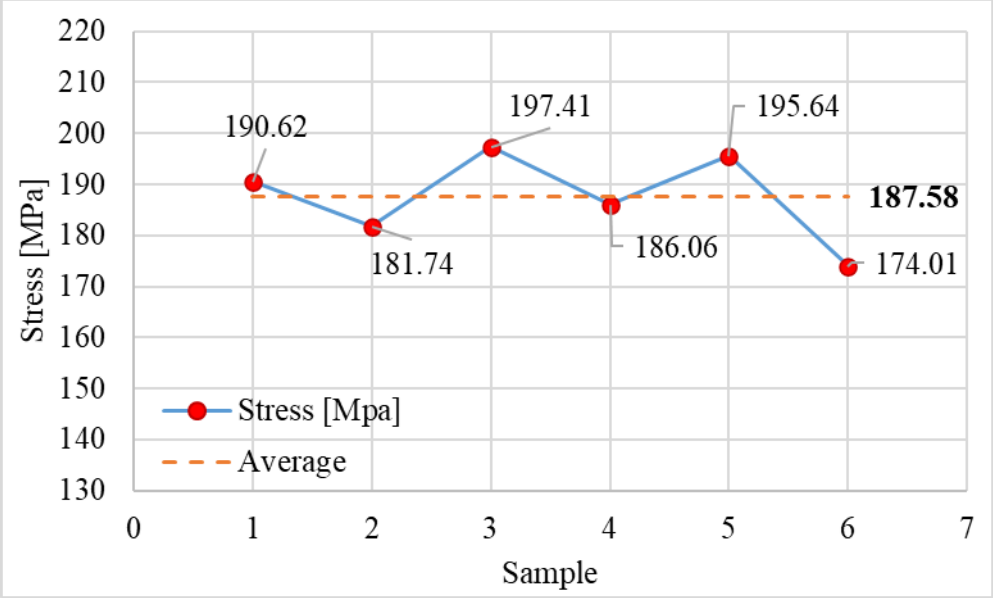


*Figure 4-13:Maximum tensile strength of sample with 0.2 mm interlayer.*

Average tensile strength of the sample with the interlayer 0.2 mm was found to be 187.58 MPa with the standard deviation of 16.15 and the average strain was 0.054 with the standard deviation of 0.33. The nature of the fracture was ductile fracture which can be explained by the SEM image of the fractured surface.

For the welded sample with 0.07 mm the maximum tensile strength ranges from 176.08 MPa to 206.66 MPa with the average tensile strength of 187.75 MPa with standard deviation of 9.11. Figure 4-7 shows the stress strain curve for the welded sample with 0.07 mm Zn interlayer.

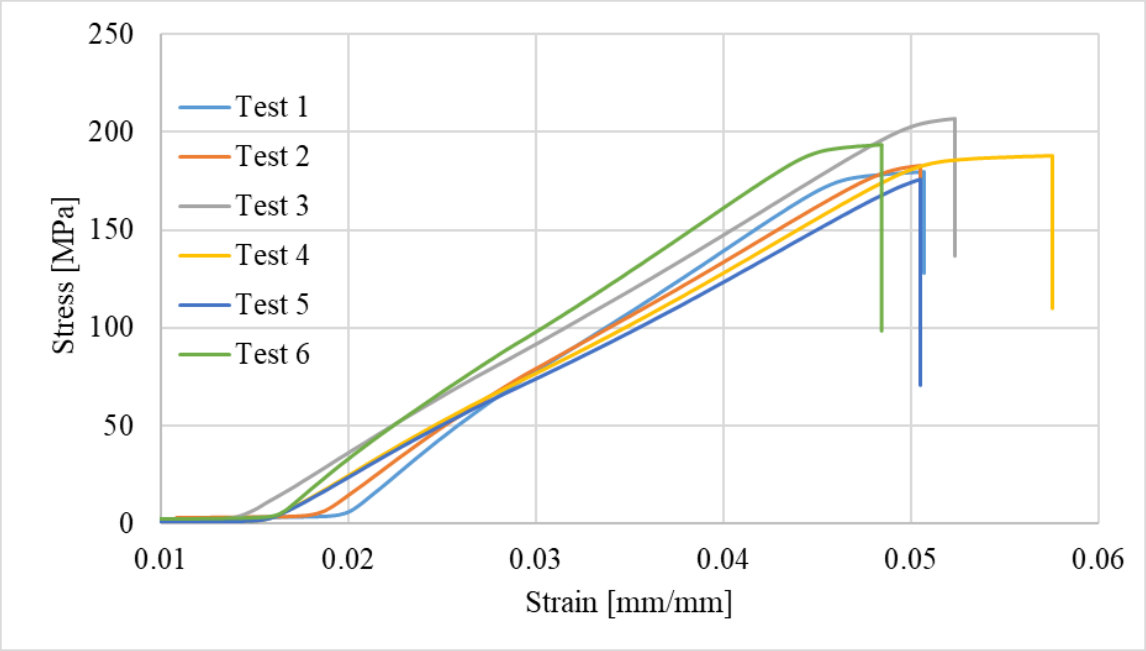


*Figure 4-14: Tensile test of welded sample with 0.07 mm Zn interlayer.*

Table 4-3 shows the maximum tensile strength for various samples and Figure 4-10 illustrates the results in line graph diagram.

*Table 4-5:Maximum Tensile strength of sample with 0.07 mm interlayer.*

| **With interlayer 0.07 mm** | | |
|---|---|---|
| **Samples** | **Stress [MPa]** | **Strain (%)** |
| **1** | 179.37 | 5.07 |
| **2** | 182.88 | 5.05 |
| **3** | 206.66 | 5.24 |
| **4** | 187.92 | 5.76 |
| **5** | 176.08 | 5.05 |
| **6** | 193.58 | 4.84 |
| **Average** | **187.75** | **5.17** |
| **SD** | **20.36** | **0.29** |

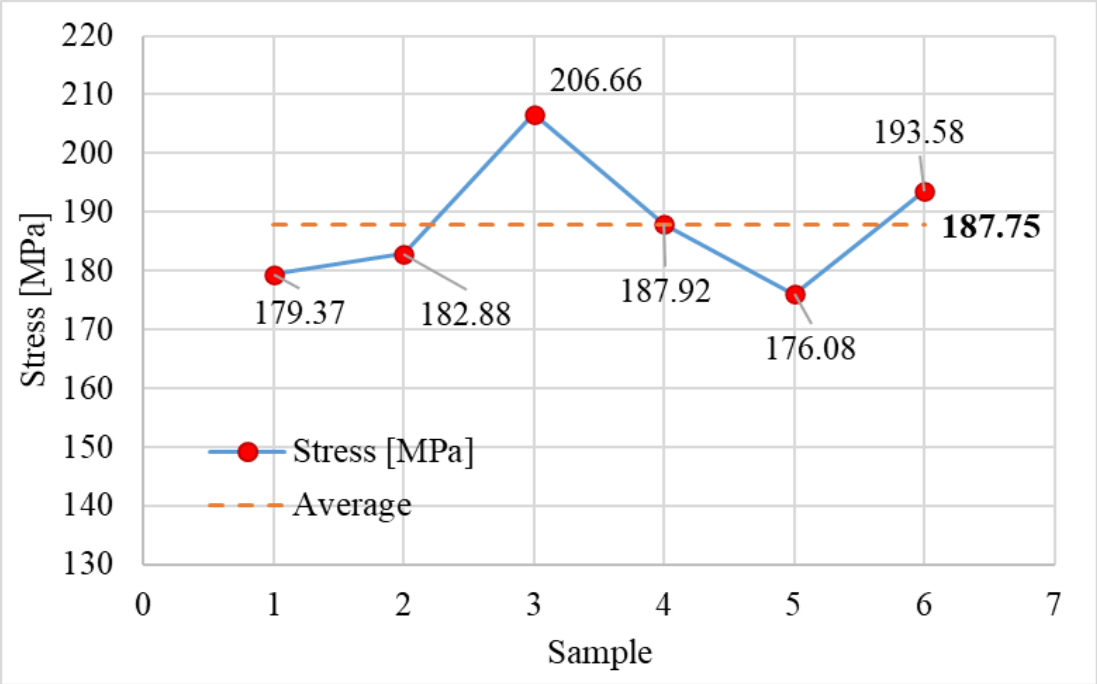


*Figure 4-15: Maximum tensile strength of sample with 0.07 mm interlayer.*

Average tensile strength of the sample with the interlayer 0.07 mm was found to be 187.75 MPa with the standard deviation of 20.36 and the average strain was 0.052 with the standard deviation of 0.29. The nature of the fracture was ductile fracture which can be explained by the SEM image of the fractured surface.

Figure 4-16 shows the comparison of stress and strain curve for the sample welded with no interlayer, with 0.07 mm Zn interlayer and 0.2mm Zn interlayer. Sample with no interlayer break earlier with the average UTS of 146.47 MPa. Sample with interlayer however has the stronger weld and does not break until they reached to about 190 MPa.

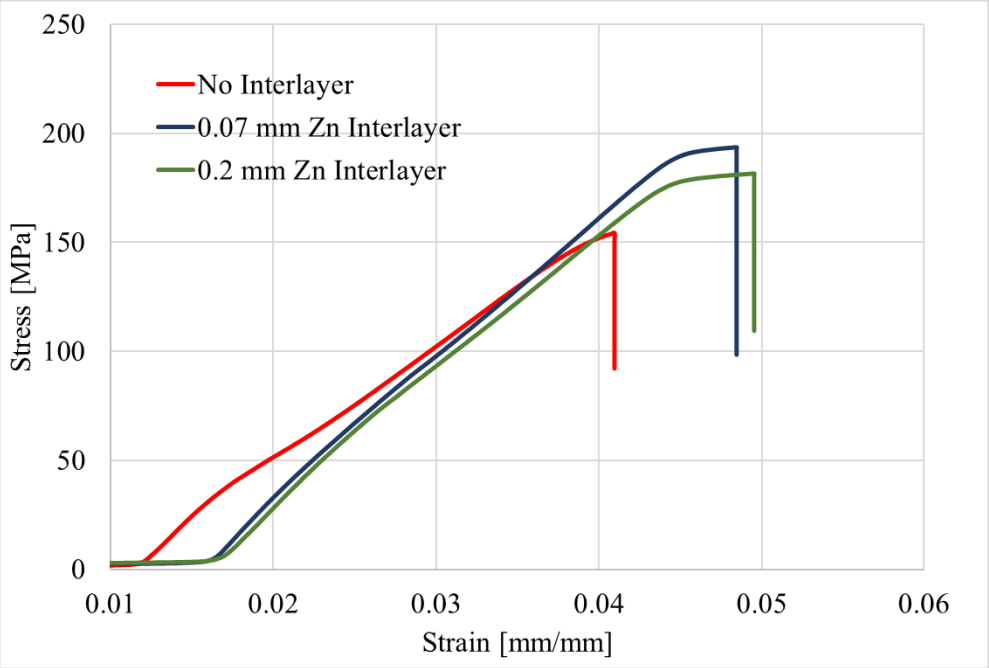


*Figure 4-16: Tensile Test comparison with and without interlayer.*

### 4.3.2 Hardness Test (Nano indentation)

Welded samples were subjected to the hardness test with nanoindentation technique. Hardness test provides valuable information about a material's mechanical properties, which is essential for ensuring product quality. Hardness test was done in different locations near the weld and on the welded junction. The hardness of the material changes as it was tested across the welding region. The hardness of the material near the welding junction tends to increase from either side. Hardness was calculated with 20 $\mu m$ interval on both the sample with and without the interlayer as shown in Figure 4-17. A total of five hardness was taken vertically at the same location to get the average hardness. Figure 4-18 shows the hardness of the sample with interlayer in the locations shown in Figure 4-17(a). Figure 4-19 shows the hardness of the sample

without interlayer on the locations shown in Figure 4-17(b). Vickers hardness of zinc is 32 HV [35].

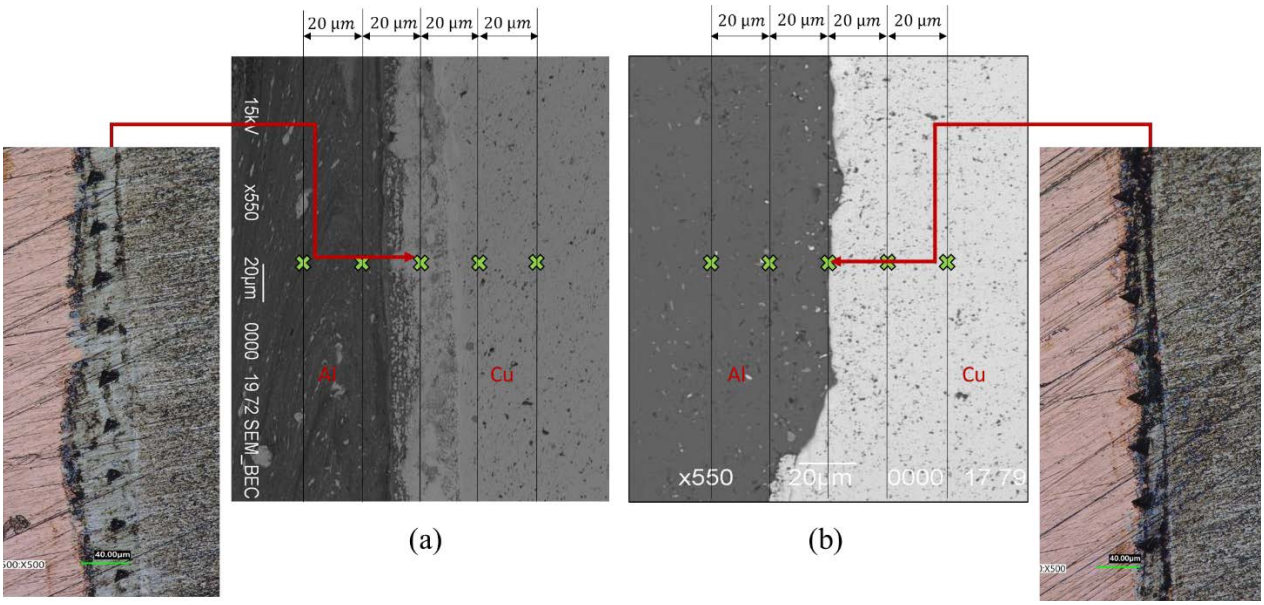


*Figure 4-17: (a) Hardness test locations on the sample with interlayer. (b) Hardness test locations on the sample without interlayer.*

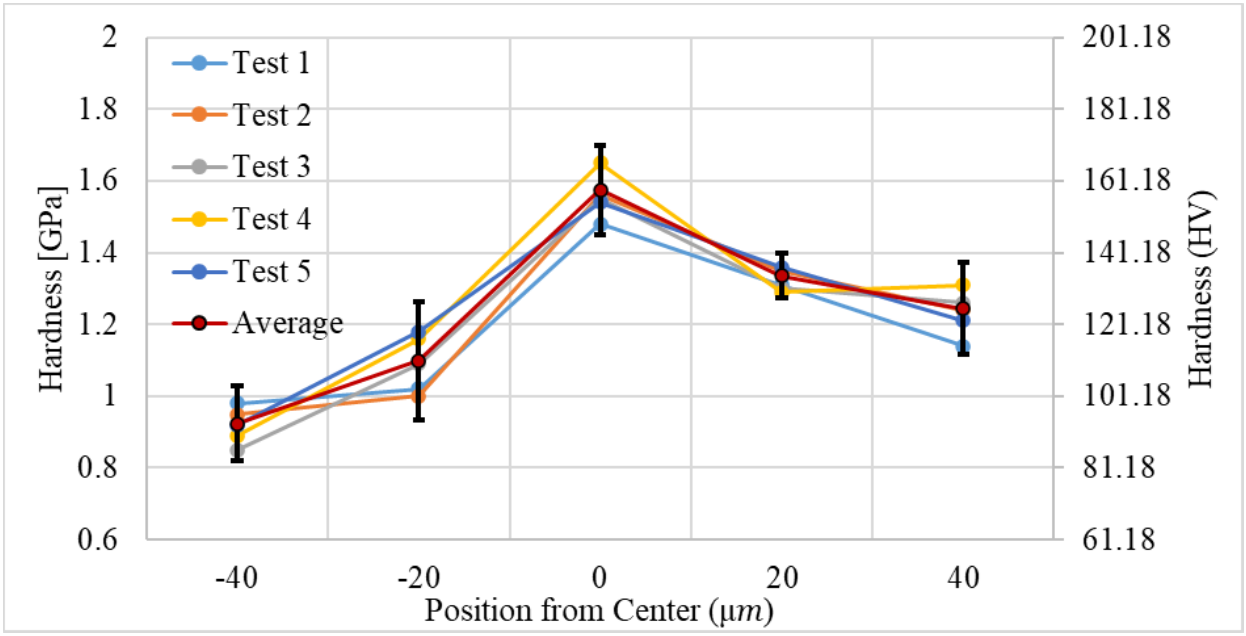


*Figure 4-18: Hardness of welded sample with interlayer (200µm) at different locations.*

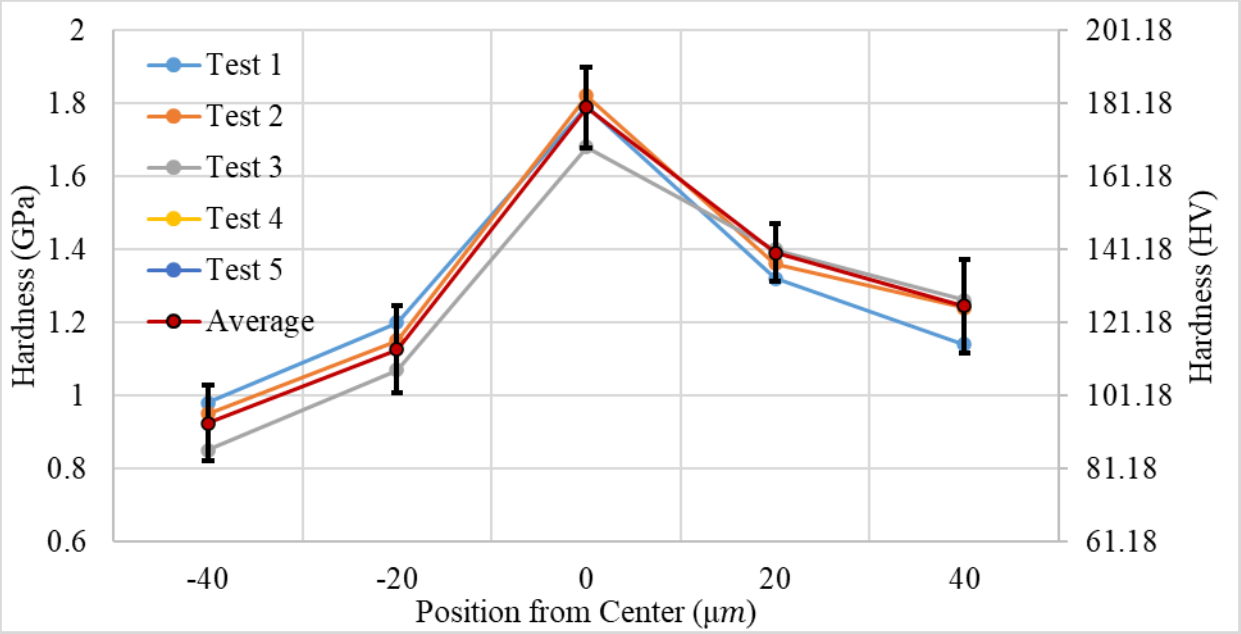


*Figure 4-19:Hardness of welded sample without interlayer at different locations.*

### 4.3.3 Thermal Analysis

Thermal Analysis was done to predict the temperature distribution on the sample based on the parameters used during the welding. This analysis takes the approach to convert mechanical energy used during the friction welding to thermal energy-which is responsible to raise the temperature. Figure 4-20 shows the 2- D temperature profile on the copper and aluminum during friction welding obtained analytically. Transient heat transfer was solved on MATLAB and the temperature changes with change in time. Figure 4-20 shows the temperature distribution after 1.5 sec of the welding. To get the 1-D plot shown in Figure 4-22, temperature across the copper from the center of the specimen was plotted. It was seen that the analysis was successfully able to predict the junction temperature. Looking at 1-D temperature profiles in Figure 4-22, it was seen that temperature obtained from analytical solution is higher than the

experimental measurements. This suggests that there is more heat transferred to the surrounding than predicted. Analytical prediction was done with various assumptions, these assumptions might also be the reason for the different temperature profile for experimental and analytical. Furthermore, the emissivity of copper and aluminum changes with temperature, which is incorporated in analytical solution, but the temperature reading from IR camera depends on the emissivity set to the software and which is constant. This also might be the reason for the difference in temperature seen in Figure 4-22. Nevertheless, both experimental and analytical temperature profiles follow a similar trend.

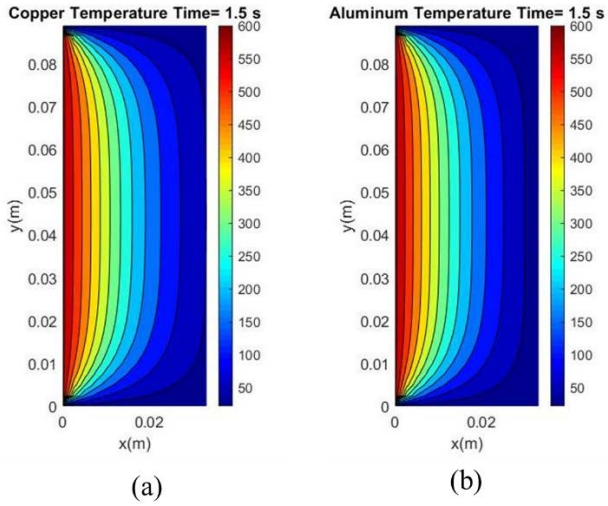


*Figure 4-20: Analytical 2-D temperature profile (a)Copper (b) Aluminum.*

Figure 4-21 shows the 2D temperature profile recorded from IR camera. FLIR camera has its own software to get the temperature profile recorded from camera called FLIR ResearchIR. On this software, emissivity is set to constant value. Although the emissivity of both copper and aluminum varies with temperature, emissivity was set to 0.2 on the software.

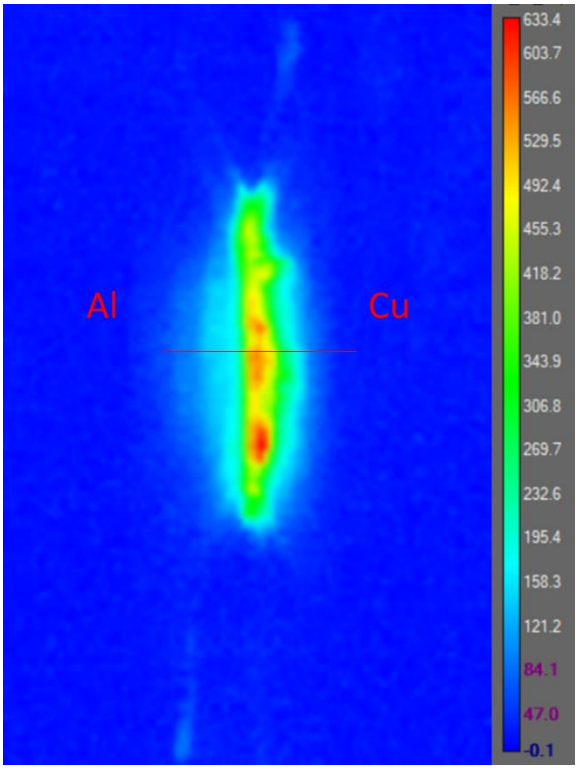


*Figure 4-21: Temperature data from IR camera.*

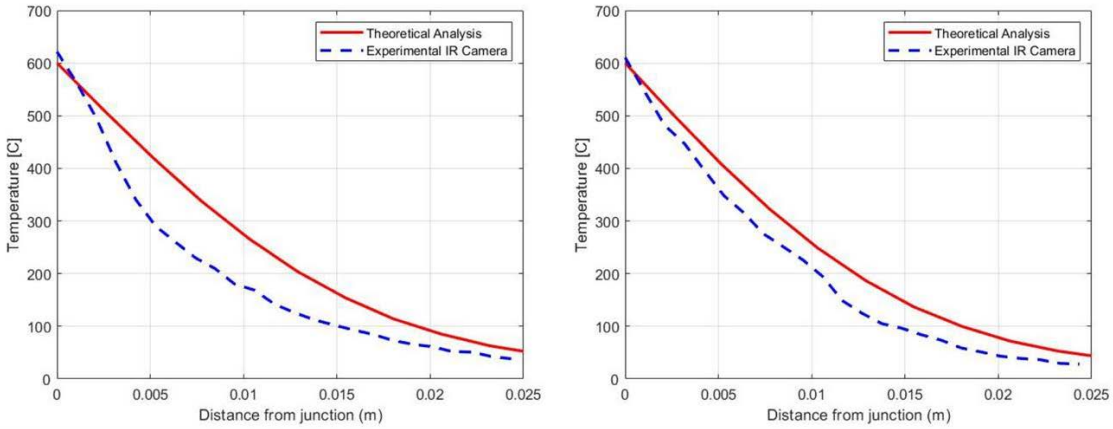


(a) (b)

*Figure 4-22: 1-D temperature profiles with Analytical and Experimental, (a) Copper (b) Aluminum.*

## 4.4 Interpretation and discussion of results

There was significant rise in UTS of the welded sample due to the introduction of Zinc interlayer while welding. With the introduction of the interlayer, there was about 28% increase in UTS which is significant improvement over the welding without the interlayer. There were some variations on the stress range of the sample which might be due to the manual human task involved in the welding process and preparation of the sample. Impurities at the interface on either of the parent metals or in Zn interlayer may have also caused the variation in UTS. Although the UTS obtained on this study was lower compared to the similar studies conducted before, this study shows a similar trend of increase in UTS with the introduction of interlayer. Figure 4-23 shows the average tensile strength of the sample with and without the interlayer.


*Figure 4-23: Average Tensile Strength of Various Sample*

Average UTS for the welded sample without the interlayer was 146.47 MPa. Weld was formed with the cracks on the junction and the fracture was brittle fracture as evident from the microstructure analysis. A similar experiment done by Yashwant et al. (2020) on Aluminum 6063 and copper with rotary friction welding obtained the maximum tensile strength of 222.7 MPa [20]. However, the experiment does not provide a comparison of the weld with and without the interlayer. M. Sahin (2009) conducted a rotary friction welding with copper and aluminum and found the maximum tensile strength of 140 MPa. This experiment compared the tensile strength with different parameters and found the optimal parameters for the highest tensile strength. Experiment by Sahin however does not provide the effect of the interlayer on the welding. A. Boucherit (2017) conducted the FSSW of Al and Cu with Zn interlayer. It was found that the presence of the Zinc interlayer inhibits the formation of brittle intermetallic compounds like $Al_4Cu_9$ at the welded interface making the weld stronger [22].

In this experiment, the Zn interlayer increases the UTS of the sample and induces some ductility on the welded interface as evident by microstructure analysis. Zn interlayer hinders the formation of brittle compounds which eliminates the crack on the welded zone and thus increases the strength.

Hardness was compared on the samples with and without the interlayer. On both the samples the hardness increases near to the junction and reaches maximum at the junction. The increase in hardness is directly related to the change in microstructure near to the junction due to the heat. Due to the heat the metal undergoes a phase transformation from its original microstructure to a new structure. This transformation can lead to the formation of various microstructural constituents, such as coarse grains, grain boundaries, and different phases.

Change in grain size and grain structure leads to the increase in hardness. As shown in Figure 4-24, average hardness for copper and aluminum is 126 HV and 94 HV respectively. The hardness measured from nano indentation machine for the aluminum 6061 was like the hardness measured in other literature while the hardness measured for the copper is slightly higher than other literature. Chee Fai Tan et al. (2009) measured the hardness of aluminum 6061-T6 and found to be 95.4 HV which is similar to the hardness measured in this experiment [31]. Jianchao Yu et al (2015), on their experiment, measured the hardness of the pure copper and found to be 107 HV which is lower than the value from this experiment [32]. As the hardness was measured in 20 $\mu m$ interval on the sample, the hardness increases towards the junction. On both Aluminum and Copper side, the average hardness increases. The hardness for aluminum reached about 111 HV-114 HV which is about 20% increase from the parent aluminum. Similarly, for copper, the hardness reached 135 HV-140 HV which is about 10% increase from the parent copper. The increase in hardness might be due to the change in grain size due to the heat created during the friction welding. At the junction, on both cases, the hardness significantly increased. Average hardness at the junction with the interlayer is 159 HV and the average hardness at the junction without the interlayer is 180 HV. Generally, brittle compounds have higher hardness than ductile materials due to the nature of their atomic or molecular structures. In brittle materials, the atomic or molecular bonds are strong and rigid. This arrangement makes it difficult for the material to undergo plastic deformation. This resistance to deformation in brittle materials results in higher hardness values [33]. On the other hand, ductile materials have more flexible atomic or molecular structure and the bonds in these materials are able to deform and stretch to a greater extent before breaking. As a result, ductile materials are generally less hard than brittle materials

[33]. Higher hardness and the tensile test fracture supports the evidence of brittle joint on the welding without the interlayer.

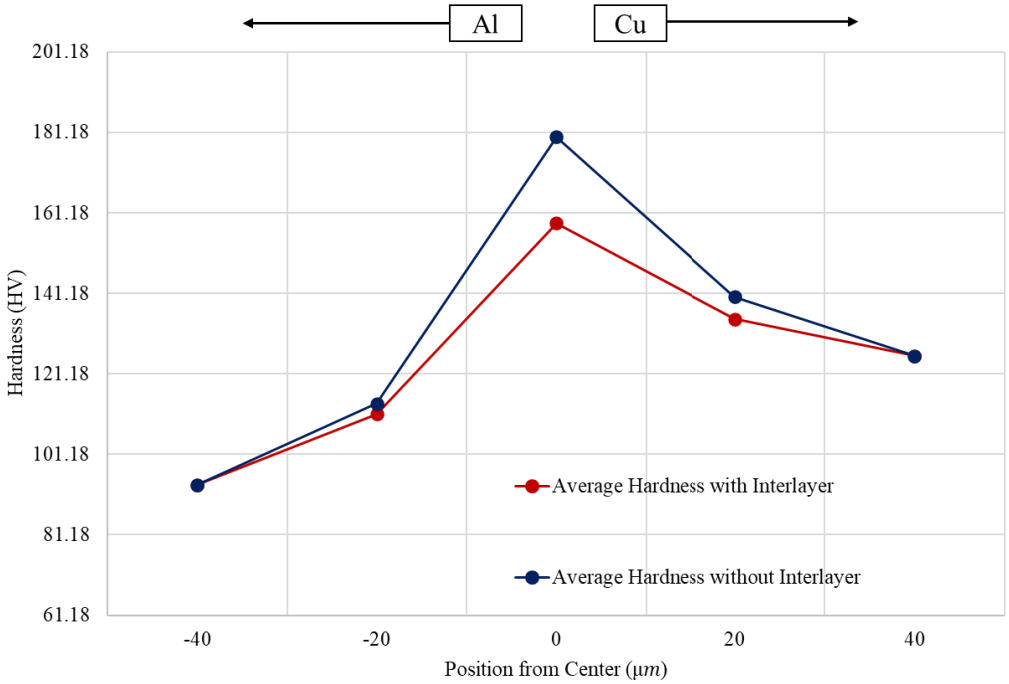


*Figure 4-24: Average hardness across the welding.*

Results of the thermal analysis were as expected. While the experiment and analytical temperature follow similar trends, there is huge difference in temperature in various points. Experimental data from all trials we not matching as well. This might be because of an error while measuring the temperature with an IR camera. For the thermal analysis, the problem was simplified with various assumptions to make the computation easier. This thermal analysis only gives the prediction of the junction temperature which is one of the important factors for the successful friction welding.

# 5 Conclusion and Recommendations

## 5.1 Summary and conclusion of the study

Successful welding of dissimilar metals- aluminum, and copper was performed, and following conclusions were obtained from the results.

1. Introduction of Zn interlayer of thickness 0.07 mm and 0.2 mm during the friction welding stops the formation of cracks at the welded junction. Which suggests the decrease of brittle intermetallic compounds while welding with Zn interlayer. Moreover, the thickness of the interlayer does not affect the strength of the weld. The result of this experiment matches the result of experiment done by Boucherit A. (2017) and his team on which they found the introduction of Zn in FSSW increase the quality of the joint and the thickness of the interlayer does not affect the strength of the weld.
2. With the introduction of the interlayer, ultimate tensile strength increases from 146.47 MPa to 187.58 MPa with 0.07mm Zn interlayer and to 187.75 MPa with 2mm Zn interlayer. There was about 28% increase in UTS which is a significant improvement over the welding without the interlayer. UTS measured on this experiment without the interlayer was comparable the UTS measured by Sahin M. (2009) on his experiment which was 140.12 MPa. However, Chapke Y. (2020) and his team were able to achieve the UTS of 222.79 MPa which is significantly larger than the UTS obtained from this experiment. Parameters plays important role in the strength of

friction welding, difference in UTS in different experiment might be due to unalike parameters used in experiments.

3. The hardness was measured at 20 μm intervals on the sample, and it was observed that the hardness increases towards the junction. On both the Aluminum and Copper sides, there was an average increase in hardness. The hardness of aluminum reached approximately 111 HV-114 HV from 94 HV, which corresponds to a 20% increase compared to the original aluminum hardness. Likewise, the hardness of copper reached 135 HV-140 HV from 126 HV, indicating a 10% increase from the original copper hardness. Hardness at the junction rose significantly on both cases with and without interlayer. Hardness at the junction without interlayer was about 180 HV and the hardness at the junction with interlayer was about 159 HV. Higher hardness value might be due to the brittle nature of the surface. Hardness measures in this experiment is slightly greater than the hardness measured by Ratkovic N R. (2017) and his team. They found hardness near the joint was 130 HV towards the copper side. However, the exact location of the measurement was not provided in the paper.
4. Microvoid coalescence, which is characteristic of ductile fracture, was seen on the fractured surface of aluminum and copper whet was welded with zinc interlayer. On the other hand, features of brittle fracture such as cleavage were seen on the fracture surface without the interlayer.
5. Thermal analysis was able to predict junction temperature based on the parameters used in welding. For the parameters used during welding the average junction temperature was about 600 ℃.

## 5.2 Recommendations for Future Research

Although successful welding was achieved between copper and aluminum, there are various fields on which there can be further improvements. Firstly, formation of oxides during the friction welding can be avoided with the introduction of inert gases like argon during welding. Decrease in the formation of oxides could help to gain more strength on the welded joints. Welding with other different interlayer thickness can be performed to see the results. Optimization of parameters with change in initial pressure, forge pressure, amplitude and frequency can be done to check for better results. For the thermal analysis, conduction of heat from the specimen to tooling can be added. All the assumptions made on this experiment can be incorporated to improve future results.

# 6 References

[1] "Metallurgy in pre-Columbian America", C.R. Biegel and J.G. Smith, 1976

[2] Shi, H., Wang, H., Yu, D., & Xia, Y. (2020). Friction welding of copper-aluminum bimetal. Materials & Design.

[3] United States Geological Survey. (2021). Copper. Retrieved from https://www.usgs.gov/centers/nmic/copper-statistics-and-information

[4] Aluminum Association. (2021). Aluminum Uses. Retrieved from https://www.aluminum.org/aluminum-uses

[5] Material properties, Retrieved from: Aluminium and Copper - Comparison - Properties - Material Properties (material-properties.org)

[6] Ahmad, R., Ahsan, Q., & Salim, M. A. (2018). Dissimilar friction stir welding of aluminum and copper: A review. Journal of Materials Processing Technology, 252, 684-699.

[7] Luo, H., Li, S., Li, X., & Li, L. (2017). Dissimilar welding of aluminum alloy to copper by laser brazing with Al-Si filler metal. Welding Journal, 96(8), 235s-242s.

[8] Ravindran, P., Shetty, D., & Kailas, S. V. (2020). Friction welding-A review. Journal of Manufacturing Processes.

[9] Singh, N. K., & Lakshmi Narayanan, A. K. (2014). Friction welding of engineering materials: a review. Materials and Manufacturing Processes, 29(12), 1419-1447. DOI: 10.1080/10426914.2014.920378

[10] Gupta, V. K., & Singh, H. (2018). Friction welding of aluminum to steel using nickel interlayer. Materials Science and Engineering: A, 720, 176-183.

[11] Zhao, L., Zeng, J., Jiang, Y., & Fan, L. (2020). Investigation of friction welding of aluminum to copper with zinc interlayer. Materials Science and Engineering.

[12] Xia, Y., Yu, D., & Wang, H. (2019). Copper-aluminum bimetal with high strength and excellent thermal conductivity prepared by friction welding. *Journal of Alloys and Compounds*.

[13] Kim, Y., Choi, I., Seo, M., Kim, J., Park, J., & Kim, J. (2019). Mechanical and tribological behavior of diamond-like carbon films with different sp3 content. Materials, 12(19), 3084. DOI: 10.3390/ma12193084

[14] Fischer-Cripps, A. C. (2002). Nanoindentation. Springer, New York, NY. doi: 10.1007/978-0-387-22458-7

[15] Nanoindentation Basic Principle. Retrieved from: https://wcnt.wisc.edu/wp-content/uploads/sites/882/2016/01/Nano_indentation.pdf

[16] Egart, M., Jankovic, B., & Srcic, S. (2016). Application of instrumented nanoindentation in preformulation studies of pharmaceutical active ingredients and excipients. DOI: 10.1515/acph-2016-0032.

[17] Yilbas B. S., Sahin A. Z., Kahraman N., & Al-Garni A. Z. (1993). Friction welding of St-Al and Al-Cu materials.

[18] Laudern A. R., & Hurricks P. L., (1973). Interaction of Lubricants and Materials. *Trans. I. Marine Eng.,* 85, 1-7.

[19] Bhamji I., Moat R. J., Preuss M., Threadgill P.L., Addison A. C., & Peel M. J., (2012). Linear Friction welding of Aluminum to Copper.

[20] Chapke Y., Kamble D., & Shaikh S. S., (2020). Friction welding of Aluminum Alloy 6063 with copper.

[21] Zhou L., Gould J. E., Lippold J. C., (2010) Dissimilar friction welding of 6061-T6 Aluminum Alloy 6063and AISI 1018 steel: Properties and microstructural characterization, *Materials and Design* 31, 2305–2311.

[22] Boucherit A., Avettand-Fenoel M.-N., & Taillard R. (2017) Effect of a Zn interlayer on dissimilar FSSW of AL and Cu. DOI: 10.1016/j.matdes.2017.03.063.

[23] Ratkovic N. R., Arsic M. D., Lazic N. V., Nikolic R. R., Hadzima B., Palcek P., & Sedmak S. A. (2016) Influence of Friction Welding Parameters on Properties of the Al-Cu Joint. DOI: 10.5937/fmet1701165R

[24] Sahin M. (2009). Joining of aluminum and copper materials with friction welding.

[25] Bozkurt, Y., & Akpınar, S. (2016). Friction Welding Process: Variables, Applications and Evaluation of Welding Strength. In Friction Stir Welding and Processing (pp. 151-189). Springer

[26] W.B. Lee, K. S. Band, S. B. Jung. Effects of intermetallic compound on the electrical and mechanical properties of friction welded Cu/Al bimetallic joints during annealing. J. Alloy Compd. 390 (2005) 212-219.

[27] Cengel A. Y., Ghajar J. A. (2015), Heat and Mass Transfer Fundamentals and Application. Published by McGraw-Hill Education, 2 Penn Plaza, New York, NY 10121.

[28] ASM Handbook, Volume 12: Fractography, ASM International, 2012.

[29] Moore P., Booth Geoff (2015), Failure modes and Analysis in metals. *The welding Engineer's Guide to Fracture and Fatigue.*

[30] OVGO data driven engineering (2015), Fractures in the SEM. Retrieved from: http://vgoinc.com/general/fractures-in-the-sem.

[31] Tan C. F. & Said M. R (2009), Effects of Hardness Test on Precipitation Hardening Aluminum Alloy 6061-T6.

[32] Yu J., Wang G., & Rong Y. (2015), Experimental Study on the Surface Integrity and Chip Formation in the Micro Cutting Process.

[33] Callister, W. D., & Rethwisch, D. G. (2014). Materials science and engineering: An introduction (9th ed.). John Wiley & Sons.

[34] Pilkey, Walter D. and Pilkey, Deborah F., "Peterson's Stress Concentration Factors," 3rd Edition

[35] Galib H. R., & Sharif A. (2015). Development of Zn-Mg Alloys as a Degradable Biomaterial. DOI: 10.7726/aac.2016.1001